Bioorganic Chemistry 99 (2020) 103844

Contents lists available at ScienceDirect

Bioorganic Chemistry

journal homepage: www.elsevier.com/locate/bioorg

Design, synthesis and biological evaluation of novel carboline-cinnamic acid hybrids as multifunctional agents for treatment of Alzheimer's disease

Qinghong Liao[a], Qi Li[c], Yifan Zhao[a], Pan Jiang[d], Yuhui Yan[d], Haopeng Sun[c], Wenyuan Liu[b], Feng Feng[a,d,*], Wei Qu[a,*]

[a] Department of Natural Medicinal Chemistry, China Pharmaceutical University, Nanjing 210009, China
[b] Department of Pharmaceutical Analysis, China Pharmaceutical University, Nanjing 210009, China
[c] Department of Medicinal Chemistry, China Pharmaceutical University, Nanjing 210009, China
[d] Jiangsu Food and Pharmaceutical Science College, Huaian 223003, China

ARTICLE INFO

Keywords:
Alzheimer's disease
Carboline-cinnamic acid hybrid
β-amyloid
Neuroprotection

ABSTRACT

Alzheimer's disease (AD) is a complex neurodegenerative disease with multiple pathological features. Multifunctional compounds able to simultaneously interact with several pathological components have been considered as a solution to treat the complex pathologies of neurodegenerative diseases. β-carboline and cinnamic acid have been extensively studied for their widespread biological effects in treatment of AD, further application is limited due to its poor solubility and high toxicity. Herein, a series of carboline-cinnamic acid hybrids was designed and synthesized to obtain new multifunctional molecules with low toxicity and good physicochemical properties. In particular, **e3** and **e12** exhibited significant inhibition of Aβ aggregation (inhibitory rate at 25 μM: 65% and 72% respectively), moderate BuChE inhibition, excellent neuroprotective effects and low neurotoxicity. Furthermore, in the AD mice model, **e3** and **e12** could restore learning and memory function to a comparable level to that of the control and did not exhibit any acute toxicity *in vivo* at a relatively high dose of 600 mg/kg. Thus, these new compounds can be further studied as multifunctional molecules for AD.

1. Introduction

Alzheimer's disease (AD) is a neurodegenerative disease, affecting more than 24 million people worldwide [1]. The World Alzheimer Report 2018 showed that 46.8 million people have been suffering from AD, and this number is expected to exceed 131.5 million in 2050 [2]. Current therapeutic options for the treatment of AD including cholinesterase inhibitors (donepezil, rivastigmine and galantamine) [3] and an *N*-methyl-D-aspartic Acid (NMDA) receptor antagonist (memantine) [4], have resulted in a modest improvement in memory and cognitive function. However, they do not prevent progressive neurodegeneration [5]. The etiology of AD remains elusive, but multiple factors, such as β-amyloid (Aβ) deposit, τ-protein hyperphosphorylation, oxidative stress, neuroinflammation and a low level of acetylcholine, likely play important roles in the development of AD [6–8].

The aggregation of Aβ may induce cytotoxicity by four mechanisms: lipid membrane permeabilization, oxidative stress, endoplasmic reticulum (ER) stress and mitochondrial dysfunction [9]. Meanwhile, in the lipid membrane, activated microglia and astrocytes by extracellular accumulation of Aβ may cause neuroinflammation [10,11]. In recent years, Aβ hypothesis is at the center of development of anti-AD drugs, and drugs targeting this system are greatly expected to be discovered. Many anti-amyloid therapies were developed, such as β- and γ-secretase inhibitors, anti-Aβ antibodies [12]. However, recent clinical trial failures cast doubt on the validity of these therapies. It has been suggested that secretase inhibitors suppress various other pathways in the brain and the peripheral tissues, exhibiting severe side effects [13,14]; anti-Aβ antibodies might be trapped in the bloodstream, allowing only limited quantities to reach the target [15]. Thus, it is promising to develop small molecules with Aβ aggregation inhibitory activity.

On the other hand, Low levels of acetylcholine affect the transmission of information in the brain, leading to cognitive decline [16], so donepezil is the most effective pharmacological agent for AD treatment. However, it is effective in reversing the symptoms for only a short period of time [17]. Studies have shown that acetylcholine (ACh) was mainly hydrolyzed by butyrylcholinesterase (BChE) during the advanced stage of AD [18]. Therefore, compounds that are able to inhibit BChE may offer an alternative role for the treatment of AD, especially in its advanced stage.

Recent evidences had demonstrated that oxidative damage in

* Corresponding authors at: Department of Natural Medicinal Chemistry, China Pharmaceutical University, Nanjing 210009, China.
E-mail addresses: fengfeng@cpu.edu.cn (F. Feng), popoqzh@126.com (W. Qu).

https://doi.org/10.1016/j.bioorg.2020.103844
Received 7 March 2020; Accepted 8 April 2020
Available online 13 April 2020

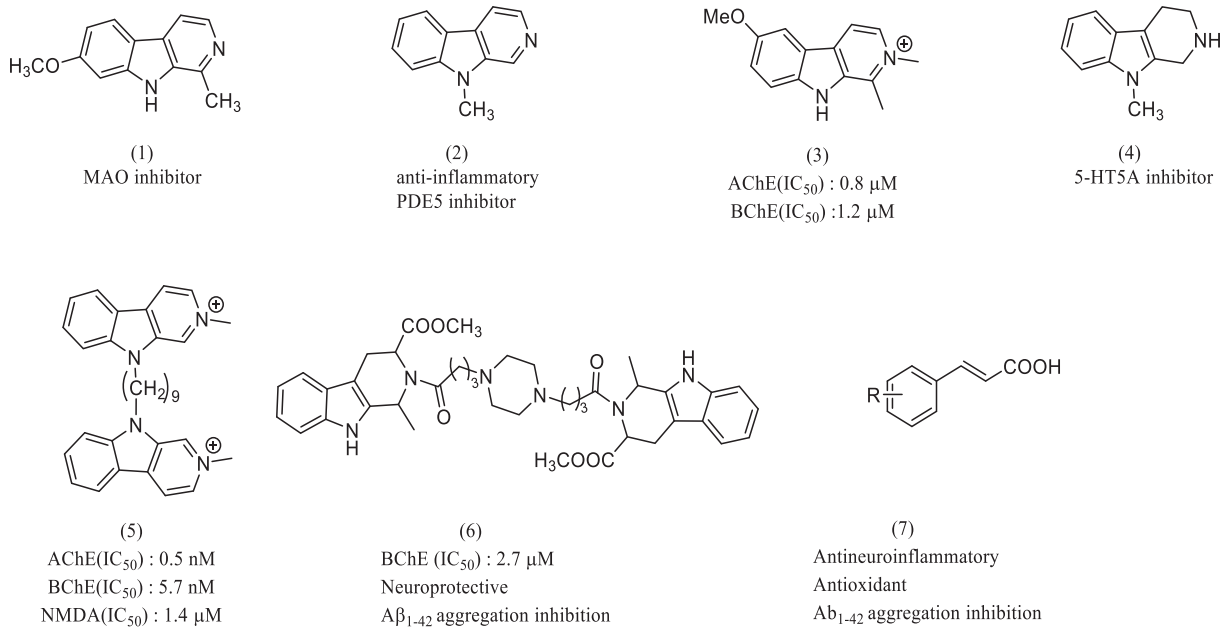

Fig. 1. Several β-carboline structures with well-known pharmacological properties.

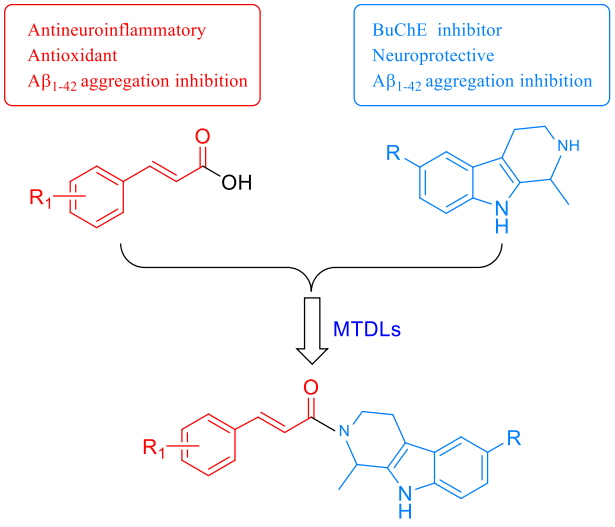

Fig. 2. Design strategy for β-carboline derivatives.

cellular structures is an event that precedes the appearance of other pathological hallmarks of AD, namely, senile plaques and neurofibrillary tangles [19]. The inflammation response triggered by AD has also been shown to induce the production of proinflammatory cytokines (such as NO, TNFα, and ROS) by microglia and resident astrocytes, which may result in neuronal cell death, and ultimately dementia [20]. Many evidences proved that antioxidants and anti-inflammatory agent could attenuate the syndrome of AD, and prevent the progression of the disease. Thus, drugs with specifically antioxidants and anti-inflammatory activity could be useful for either the prevention or the treatment of AD.

Due to the multifactorial nature of AD, multifunctional ligands are supposed to exhibit promising therapeutic effects, therefore, it is considered to be an important strategy for the development of anti-AD drugs [21–23]. Some researches showed that about 84% approved drugs for CNS diseases are NPs or NP-inspired, and interestingly, 20 NP structures provided more than 400 clinically approved CNS drugs [24]. β-carboline, a multifunctional natural products with a pyrido [3,4-*b*] indoles structure [25–27], have been extensively studied for its wide range of biological effects [28,29]. Several evidences (Fig. 1) have suggested that β-carboline analogs function as anti-AD agents through inhibition of cholinesterase [30], inhibition of monoamine oxidase (MAO) [31,32], anti-inflammation [33,34] and anti-aggregation [35]. Furthermore, the studies indicated that bivalent β-carbolines analogs exhibited more potent AChE inhibitory activities with IC_{50} values in the nanomolar range [36,37]. Evidences showed that bivalent β-carboline derivatives exhibited good multifunctional activities such as ChEs inhibition, $A\beta_{1-42}$ aggregation inhibition and neuroprotection [38]. However, further application of bivalent β-carboline derivatives is limited due to its poor solubility and high toxicity [38]. Other natural compounds, such as cinnamic acids, have also been studied extensively as anti-AD agents because of their anti-neuroinflammatory properties [39] and ability to inhibit Aβ aggregation [40] by scavenging oxidants [41,42]. Thus, β-carboline and cinnamic acid were considered as suitable multifunctional fragments.

Considering the poor druggability of carboxylic acids, we intended to replace carboxyl with other structures. Due to the poor physicochemical properties and safety of bivalent β-carboline derivatives, in the present study, we fused β-carboline with another natural product cinnamic acid, to obtain a new kind of heterogenous dimer with low toxicity and molecular weight, good molecular planarity and physicochemical properties (Fig. 2). We hypothesize that carboline-cinnamic acid hybrids could show complementary activities of two fragments.

2. Results and discussion

2.1. Chemistry

The synthetic route for the new β-carboline derivatives is shown in Schemes 1. Using the substituted tryptamine as a raw material, the target compounds **2a**, **2b** (tetrahydro-β-carboline) were obtained by reaction with excess aldehyde (dropwisein ice bath) in a solution of about 5% trifluoroacetic acid (pH = 2–3) in dichloromethane. Commercially available substituted cinnamic acid reacted with dichlorosulfoxide at 80 °C to give **d1–d9**. Compounds **d1–d9** were reacted with different tetrahydro-β-carboline analogs in the presence of Et_3N to provide the target compounds **e1–e18**.

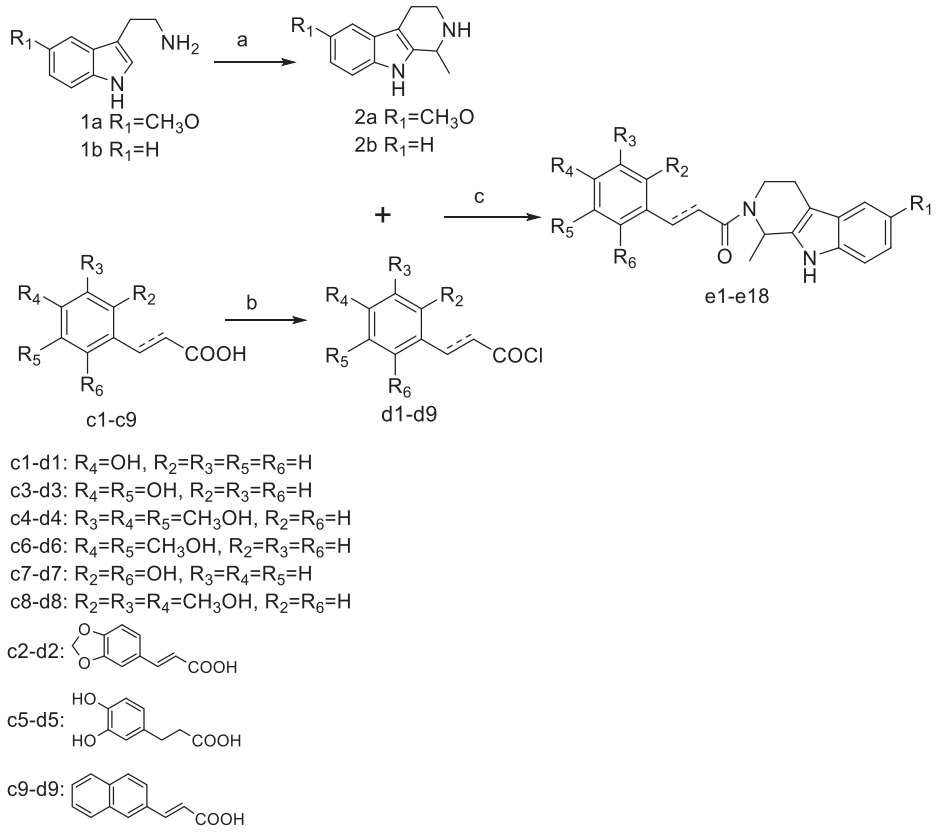

Scheme 1. Synthesis of **e1**-**e18.** [a]Reagents and conditions: (a) acetaldehyde, DCM and 5% TFA, rt, 24 h; (b) $SOCl_2$, reflux, 4 h; (c) dry THF, Et_3N, rt, 12 h.

2.2. Inhibition of self-mediated $A\beta_{1-42}$ aggregation

The inhibitory activities of β-carboline derivatives against self-mediated $A\beta_{1-42}$ aggregation were evaluated using a thioflavin T (ThT) fluorescence assay [43–45]. using resveratrol as the positive control [46]. None of the test compounds exhibited interfering signals under the experimental conditions. The data were summarized in Table 1. The results indicated that **caffeic acid** and compounds **1a** and **1b** presented low inhibitory activities, while **e3** and **e12** were the most potent inhibitors of $A\beta_{1-42}$ aggregation among the series of compounds featuring a 3,4-dihydroxy group on the A ring, which proved the rationality of our designed strategy. The methoxy-substituted compounds were less active than the hydroxy-substituted group, indicating the importance of hydroxy substitution for inhibiting Aβ aggregation. The different position of methoxy group has little effect on the activity of the compound. In addition, **e5** and **e14**, with reduced double bonds, gave slightly weaker inhibitory activities than **e3** and **e12**. Compounds **e9** and **e18** with naphthalene rings also exhibited good inhibitory activities (54.3% and 58.2%, respectively). We next conducted docking studies of **e12** with amyloid forming peptide KLVFFA (PDB code 3OVJ) by using the CDOCKER program embedded in Discovery Studio (DS) 2019. The results showed that **e12** could embedded in β-sheet structure and mainly exhibited hydrophobic and hydrogen-bonding interactions, indicating that the β-carboline derivatives could inhibit $A\beta_{1-42}$ aggregation by hindering the formation of the β-sheet structure (Fig. 3**A**). We could draw conclusions that polyhydroxy substitution, good molecular planarity and a large conjugated system are prerequisite for inhibiting Aβ aggregation.

2.3. Inhibition of cholinesterase (ChE) activities

Cholinergic dysfunction leads to cognitive decline, and a promising approach to the treatment of AD is the usage of natural products with the ability to increase acetylcholine levels [47]. Research shows that BuChE inhibitors are more durable and stable, and have unique advantages in the treatment of moderate or severe AD [48]. To further study the multi-biological profile of the target compounds, the abilities of the most promising compounds **e3** and **e12** to inhibit AChE and BuChE were evaluated [49]. As shown in the Table 2., **e3** and **e12** exhibited moderate BuChE inhibitory activities and good selectivity, which were higher than the monomeric compounds such as **caffeic acid**, **1a** and **1b**. From the interaction mode of **e12** for BuChE(PDB: 4TPK), the carboline core interacts with Tyr332 through a π-π stacking contact. The N atom of the indole ring interacts with Asp70 through a hydrogen bond. The phenyl ring of the cinnamic acid moiety is engaged in π-π interactions with Trp82. Two hydroxyl group of the cinnamic acid moiety forms two hydrogen bond with Gly115 (Fig. 3**B**). Therefore, **e12** can better occupy the active site of BChE, leading to its great BChE inhibitory activities and selectivity.

2.4. Cytotoxicity of synthetic compounds in PC12, SH-SY5Y, BV-2, HT22, L02 cells

To investigate the safety profile of these synthetic compounds, we determined the potential cytotoxic effects of compounds **e3** and **e12** on five cell lines (PC12, SH-SY5Y, BV-2, HT22, L02). After exposing the cells to these compounds for 24 h, the cell viability was evaluated by 3-(4,5-dimethylthiazol-2-yl)-2,5-diphenyltetrazolium (MTT) assay. All cells could be well tolerated at a relatively high dose (Detailed IC_{50} values were presented in Table S1). The results demonstrated that there was no obvious death of five cell lines at 25 μM of **e3** and **e12**, meaning that these compounds were not neurotoxic when applied at these concentrations (Fig. 4).

Table 1
Inhibition of $A\beta_{1-42}$ aggregation of β-carboline derivatives **e1**-**e18**.

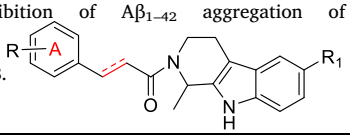

Cpd.	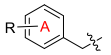	R_1	$A\beta_{1-42}$ aggregation inhibition (%)[a]
e1	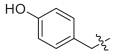	Methoxyl	18.65 ± 5.63
e2	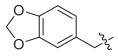	Methoxyl	32.09 ± 1.16
e3	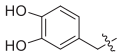	Methoxyl	65.49 ± 2.25
e4	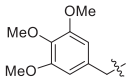	Methoxyl	20.19 ± 4.70
e5	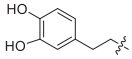	Methoxyl	58.64 ± 0.68
e6	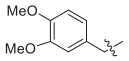	Methoxyl	35.33 ± 0.70
e7		Methoxyl	31.15 ± 1.17
e8	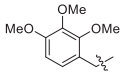	Methoxyl	21.93 ± 0.76
e9	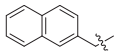	Methoxyl	54.30 ± 0.68
e10	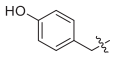	Hydrogen	23.72 ± 2.45
e11	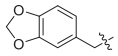	Hydrogen	21.99 ± 0.72
e12	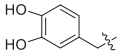	Hydrogen	72.51 ± 0.84
e13	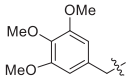	Hydrogen	31.87 ± 2.33
e14	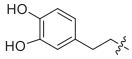	Hydrogen	58.41 ± 3.21
e15	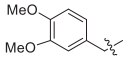	Hydrogen	27.03 ± 1.80
e16		Hydrogen	21.45 ± 0.29
e17	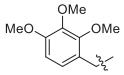	Hydrogen	31.99 ± 0.96
e18	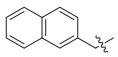	Hydrogen	58.19 ± 1.47
1a	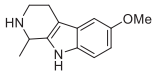	–	n.a.[b]
1b	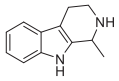	–	n.a.[b]
Caffeic acid	–	–	31.48 ± 0.83

Table 1 (*continued*)

Cpd.	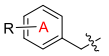	R_1	$A\beta_{1-42}$ aggregation inhibition (%)[a]
Resveratrol	–	–	43.48 ± 2.26

[a] The thioflavin-T fluorescence method was used. The values are expressed as the mean ± SEM of at least three independent measurements. All values were obtained at a compound concentration of 20 μM.
[b] n.a. means no activity.

2.5. Neuroprotection of compounds on H2O2-induced cell insults

Oxidative stress is an important pathogenesis of AD, which can be induced by H_2O_2 and cause cell damage [50]. Therefore, we evaluated the neuroprotective effects of the **e3** and **e12** on H_2O_2-induced cells insults [51]. As expected, the treatment of PC12 and SH-SY5Y cells with H_2O_2 for 24 h significantly reduced cell viability. Meanwhile, the survival of H_2O_2-treated cells obviously increased following pretreatment with **e3** or **e12** in a dose-dependent manner. The compounds even completely reversed this damage at 15 μM. These data indicated that **e3** and **e12** were protective agents against H_2O_2-induced cell death in human PC12 and SH-SY5Y cells (Fig. 5).

2.6. Effect of compounds on OA-induced cytotoxicity

One of the pathological features of the brains of AD patients, neurofibrillary tangles (NFTs) are mainly caused by tau hyperphosphorylation and aggregation [52,53]. Therefore, we investigated the protective effect of these molecules on okadaic acid (OA, a tau protein hyperphosphorylation inducer) induced cells toxicity. PC12 and SH-SY5Y cells were incubated with OA and the selected compounds for 48 h, and the cell viability was tested using MTT [54]. As shown in Fig. 6, OA significantly reduced the cell viability, while **e3** and **e12** treatment moderately increased the viability of the cells. Therefor **e3** and **e12** could reduce PC12 and SH-SY5Y cytotoxicity induced by OA.

2.7. Effect of compounds on $A\beta_{1-42}$-induced cells toxicity

Senile plaque, another histopathological hallmark of AD, are mainly due to the accumulation of amyloid β peptides [55]. We have explored these compounds could remarkably inhibit $A\beta_{1-42}$ aggregation, herein, the neuroprotective role of compounds on $A\beta_{1-42}$-dependent cell death was investigated [56]. The results indicated that $A\beta_{1-42}$ (30 μM) obviously induced a sharp decline in cell viability, and compounds **e3** and **e12** could protect nerve cell from $A\beta_{1-42}$-mediated neurotoxicity (Fig. 7).

2.8. Effect of compounds on LPS-induced ROS production

Microglia-mediated neuroinflammation is an important contributor to the pathogenesis of neurodegenerative diseases [57]. Activated microglia produces toxic inflammatory mediators, such as NO, cytokines and ROS, ultimately resulting in the loss and death of neurons [58]. To investigate the anti-neuroinflammatory effects of hit compounds, BV-2 cells were stimulated with Lipopolysaccharide (LPS) (2.5 mg/L), and the secretion of ROS was measured with the fluorescent dye H2DCFDA [59,60]. The significant increasing in fluorescence intensity of BV-2 cells could be clearly observed after 24 h treatment with LPS, while that of LPS-induced cells remarkably reduced following pretreatment with **e3** or **e12** (Fig. S1). As shown in Fig. 8, the results showed that **e3** and **e12** suppressed ROS released in LPS-stimulated BV-2 cells. Hence, molecules bearing the radical scavenging phenol and β-carboline scaffold could reduce ROS-induced cell death, and result in alleviating neuroinflammatory process in the brain during AD.

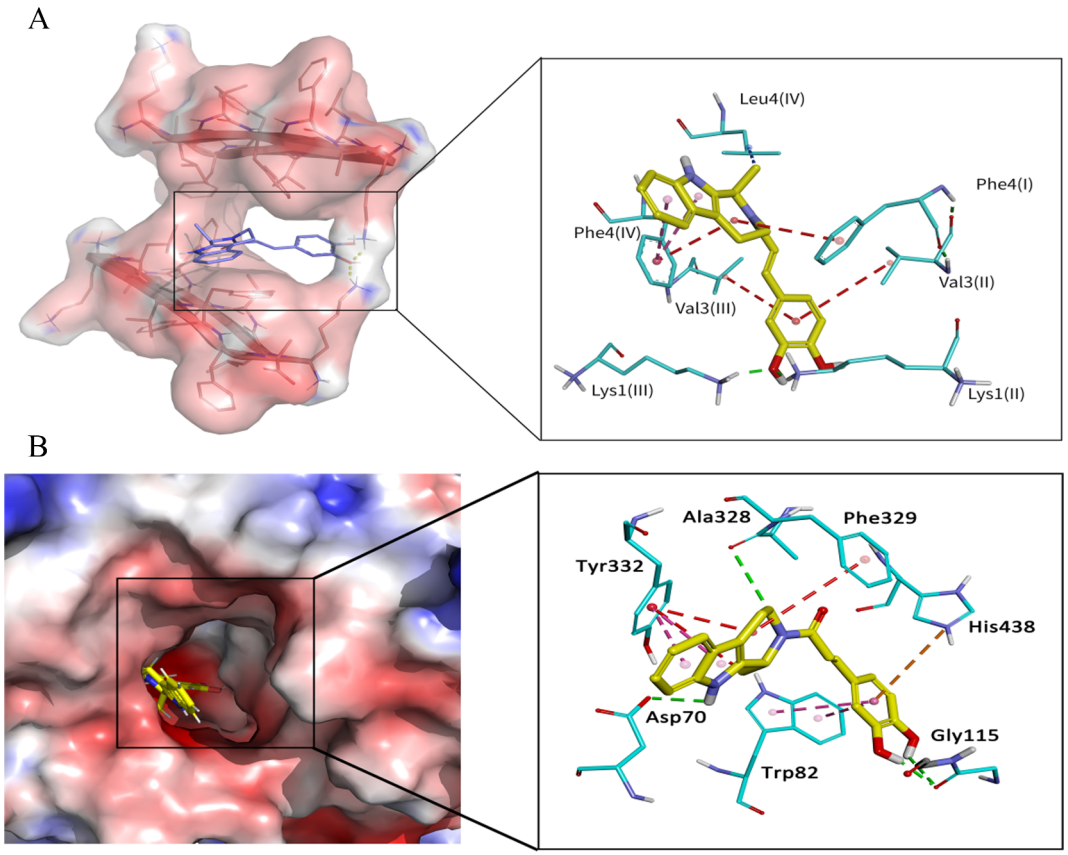

Fig. 3. (A) Binding modes of e12 with amyloid forming peptide KLVFFA (left) and an interaction map (right) displaying the binding and interactions of compound **e12**. (B) The BChE active site cavity (left) and interaction map (right) displaying the binding and interactions of compound **e12**. Color coding: green: hydrogen bond; purple: π–π stacking; red: π–Alkyl; orange: π–Cation. (For interpretation of the references to colour in this figure legend, the reader is referred to the web version of this article.)

2.9. Predicted the ADMET and physicochemical properties of compounds candidates

The ADMET and physicochemical properties of active compounds **e3** and **e12** were calculated by using QikProp and Discovery Studio 2019 prior to performing animal assays. CYP2*D6* is mainly expressed in the liver and highly expressed in the central nervous system, including substantia nigra. As reported in Table 3, **e3 and e12** displayed no inhibition of CYP2*D6* [61,62] indicating an unlikely adverse effect on liver. Moreover, compounds exhibited moderate blood-brain barrier permeability and high oral absorption. The selected compounds presented a favorable drug-like profile with no violation of either Lipinski's

Table 2
ChE Inhibitory Activities of compounds.

Cpd.		R_1	IC_{50} ± SEM (μM)[a]	
			AChE[b]	BuChE[c]
e3	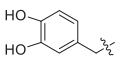	Methoxyl	75.32 ± 9.38	6.47 ± 4.17
e12	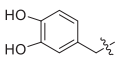	Hydrogen	21.29 ± 3.63	1.32 ± 0.85
1a	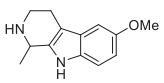	–	> 100	74.81 ± 9.45
1b	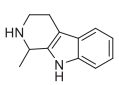	–	> 100	90.22 ± 8.42
Caffeic acid	–	–	n.a.[d]	n.a.[d]
Donepezil	–	–	0.05 ± 0.01	3.15 ± 0.65

[a] IC_{50}, inhibitor concentration (means ± SEM of three independent experiments) for 50% inactivation of AChE and BuChE.
[b] AChE from electric eel was used.
[c] BuChE from equine serum was used.
[d] n.a. means no activity.

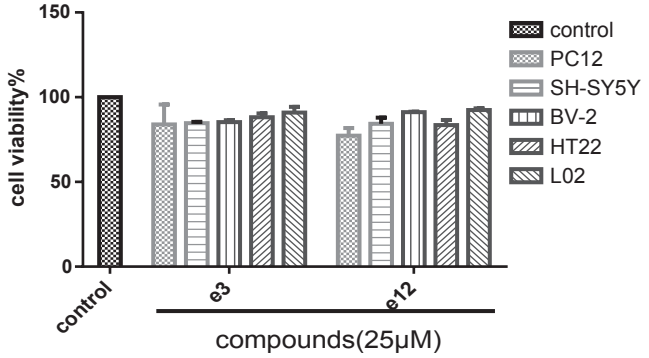

Fig. 4. Effects of compounds on the viability of PC12, SH-SY5Y, BV-2, HT22 and L02 cells. The cells were incubated with the indicated concentrations (25 μM) of the test compounds for 24 h before evaluated by the MTT assay Cell viabilities are presented as mean ± SEM from three independent experiments.

rule of five or Jorgensen's rule of three.

2.10. In vivo activity

To evaluate the *in vivo* activities of synthesized compounds, we used Morris water maze and Y maze to assess learning and memory function in an acute AD mice model, where Aβ oligomer was directly injected into the brains of normal mice to induce acute neurotoxicity [63,64]. After orally administrating compounds **e3** and **e12** for two weeks, we performed Y maze and Morris water maze to measure cognitive improvement of AD mice. As described in Fig. 9**A**, none of the blank control groups (oral for Saline and hippocampal injection for Saline) significantly affected the mouse cognitive function. Hippocampal injection of the oligomerized $A\beta_{1-42}$ peptide led to spontaneous alternation deficits compared to the sham-operation group. Donepezil showed prevention against the $A\beta_{1-42}$-induced alternation deficit at 15 mg/kg, and **e3** and **e12** could also remarkably increase alternation percentage at 15 mg/kg oral doses.

Subsequently, Morris water maze test was conducted to evaluate the learning and memory abilities. The sham-operation group remained no difference from the control group, and it was clear that administration of oligomerized $A\beta_{1-42}$ led to a prominent delay of the latency to target, compared to the sham-operation group. Donepezil exhibited much improved cognitive function in the ICR mice, as the latency to target obviously reduced compared to model. Besides, the mice treated with **e3** or **e12** both demonstrated a favorable amelioration of the cognitive and memory functions compared to the model group (Fig. 9B). The same conclusion was derived from the confusion degree of the trajectories of the mice in each group (Fig. 9C). In additional, neither the intragastric administration nor the hippocampal injection of the peptide affected the body weight of mice during the two-week-therapy, showing a good *in vivo* safety of the two candidates (Fig. S2).

In summary, the representative **e3** and **e12** showed auspicious effects on diverse investigated behavioral parameters, and the results may be attributed to the anti-aggregation, antioxidant or other neuroprotective activities of the compounds.

2.11. Assessment of acute toxicity

The acute toxicity trials of **e3** and **e12** were carried out in adult ICR mice (male mice, 8–10 weeks old, weight 18–20 g). All the mice remained alive and abnormal behavior after intragastric administration of **e3** and **e12** at doses of 200 mg/kg and 600 mg/kg (n = 5 per group). Furthermore, from the first 4 h through 14 days after administration, there was no obvious behavior abnormality compared to the control group (Fig. S3). All the results support these natural product analogues as multifunctional molecule with high efficiency, low toxicity, and good oral bioavailability.

3. Conclusion

Based on the various biological activities of carboline derivatives, a series of carboline-cinnamic acid heterogenous dimer were designed and synthesized as multifunctional agents for the treatment of AD in this study. Among the synthesized compounds, **e3** and **e12** exhibited significant inhibition of Aβ aggregation, moderate BuChE inhibition, excellent neuroprotective effects and low neurotoxicity. Furthermore, orally administrating **e3** and **e12** to AD model mice, could restore learning and memory function to a comparative level to that of the control without acute toxicity in mice at doses up to 600 mg/kg. The outcomes above verified **e3** and **e12** promising multifunctional agents in the drug discovery process against AD.

4. Experimental section

4.1. Chemistry

^{1}H and ^{13}C NMR spectra were recorded on a Brüker 300, 400 and 500 MHz spectrometer at 298 T and referenced to TMS. MS spectra data were obtained on an Agilent-6210 LC-MS spectrometer. Thin-layer chromatography was carried out on silica gel GF/UV 254 supported by

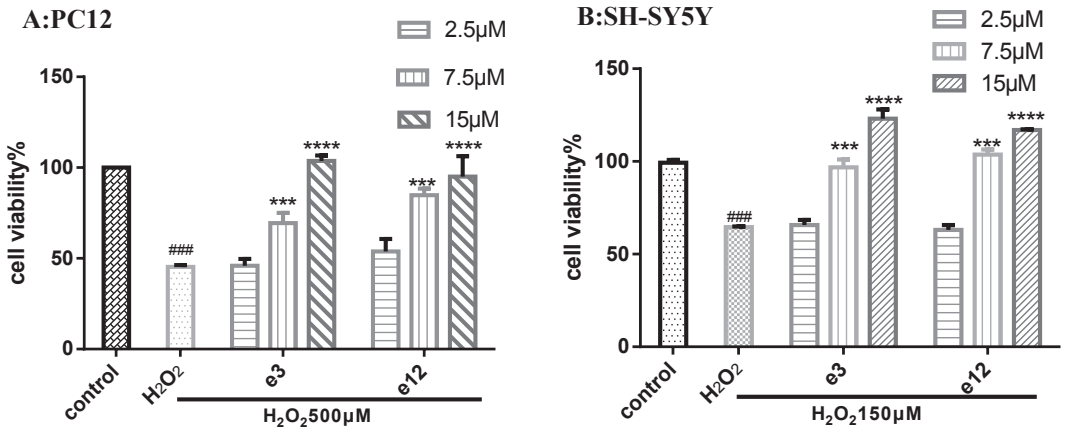

Fig. 5. Compounds hindered H_2O_2-induced cell damage in PC12 and SH-SY5Y cells. (A) PC12 cells were pre-treated with compounds (2.5–15 μM) for 2 h and then incubated with H_2O_2 (500 μM) for 24 h before MTT assay was performed. (B) SH-SY5Y cells were pre-treated with compounds (2.5–15 μM) for 2 h and then incubated with H_2O_2 (150 μM) for 24 h before MTT assay was performed. All data are expressed as mean ± SEM of three independent experiments. $^{\#\#\#\#}p < 0.0001$ vs. control; $^{***}p < 0.001$, $^{****}p < 0.0001$ vs H_2O_2.

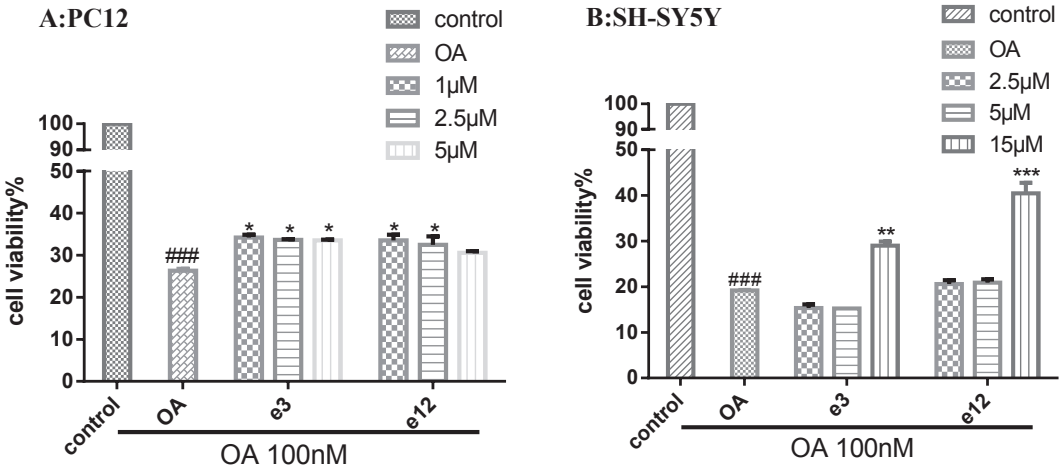

Fig. 6. Compounds alleviates OA induced cell toxicity in PC12 and SH-SY5Y cells. (A) PC12 cells were pre-treated with compounds (1–5 μM) for 2 h and then incubated with OA (100 nM) for 24 h before MTT assay was performed. (B) SH-SY5Y cells were pre-treated with compounds (2.5–15 μM) for 2 h and then incubated with OA (100 nM) for 24 h before MTT assay was performed. All data are expressed as mean ± SEM of three independent experiments. $^{\#\#\#\#}p < 0.0001$ vs. control; $^{*}p < 0.05$, $^{**}p < 0.01$, $^{***}p < 0.001$vs. OA.

glass plate, and the chromatograms were performed on silica gel (200–300 mesh) visualized under UV light at 254 and 365 nm.

4.1.1. General procedure I

Compounds **2a**, **2b** were synthesized according to Pictet-Spengler reaction [65]. Tryptamine (1 equiv) was dissolved in CH_2Cl_2 and cooled to 0 ˚C in an ice bath. To this solution, trifluoroacetic acid (1.5 equiv) was added dropwise and the mixture was stirred at 0 ˚C for about 0.5 h. Then acetaldehyde (4 equiv) was added to this solution and the resulting mixture was stirred at room temperature for 24 h. The complete reaction was monitored by TLC layer and the reaction mixture was then basified with dilute NH_4OH solution and extracted with CH_2Cl_2. The solvents were removed under reduced pressure to obtain the crude product, which was purified by column chromatography.

4.1.2. General procedure II

Substituted cinnamic acid (1 equiv) was dissolved in $SOCl_2$ (10 equiv) and refluxed for 4 h. The solvents were removed under reduced pressure to obtain the substituted cinnamoyl chlorides.

4.1.3. General procedure III

2a or **2b** was added to a mixture of substituted cinnamoyl chloride

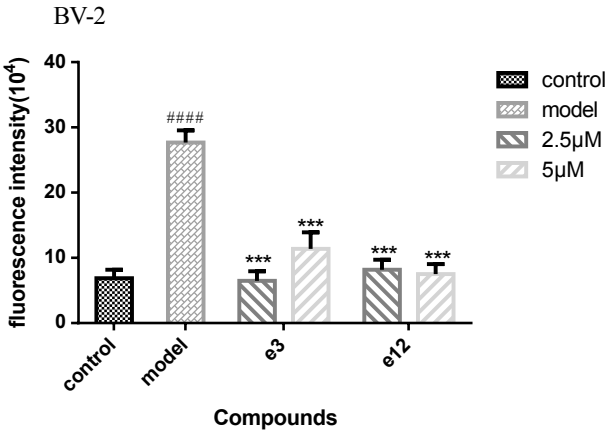

Fig. 8. Compounds lessened LPS-induced ROS production in BV-2 cells. BV-2 cells were pre-treated with compounds (2.5–5 μM) for 0.5 h and then incubated with LPS (2.5 mg/L) for 24 h. Intracellular ROS production levels were then measured with the fluorescent dye H2DCFDA. Bars correspond to the fluorescence intensity and are the means ± SEM of three independent experiments. $^{\#\#\#\#}p < 0.0001$ vs. control; $^{***}p < 0.001$vs. model.

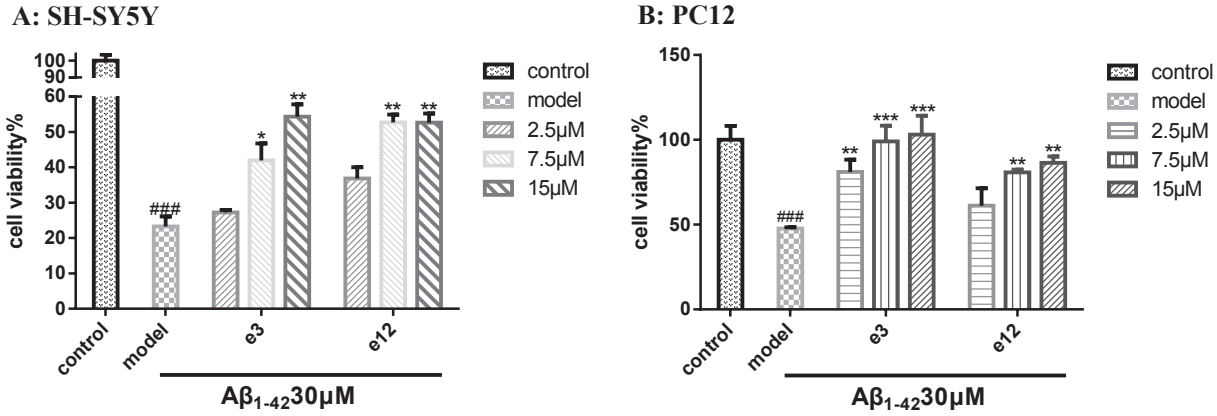

Fig. 7. Compounds protected against $A\beta_{1-42}$ -induced cell toxicity in PC12 and SH-SY5Y cells. SH-SY5Y (A) and PC12 (B) cells were pre-treated with compounds (2.5–15 μM) for 2 h and then incubated with $A\beta_{1-42}$ (30 μM, Oligomer) for 48 h before MTT assay was performed. All data are expressed as mean ± SEM of three independent experiments. $^{\#\#\#}p < 0.001$ vs. control; $^{**}p < 0.01$, $^{***}p < 0.001$vs. model.

Table 3
Calculated Physicochemical Properties for Selected Compounds Using QikProp and Discovery Studio 3.0.

Calculated properties	Content	e3	e12	Guideline
CYP2*D6* inhibition	–	False	False	–
ADMET_BBB_Level	BBB permeability	2	2	Moderate
Percent Human Oral Absorption	Human oral absorption	94.126	93.736	> 80%, high; < 25%, poor
QPlogPo/w	Octanol/water partition coefficient	3.426	3.404	−2–6.5
QPlogS	Aqueous solubility	−5.236	−5.25	−6.5–0.5
QPlogBB	Brain/blood partition coefficient	−1.256	−1.219	−3.0–1.2
metab	Number of possible metabolic reactions	5	4	1–8
SASA	Total solvent accessible surface area	251.648	171.398	300–1000
QPlogHERG	IC_{50} value for blockage of HERG K^+ channels	−5.874	−6.185	< -5
QPPCaco	Caco-2 cell permeability	429.22	414.993	> 500,great; < 25%, poor

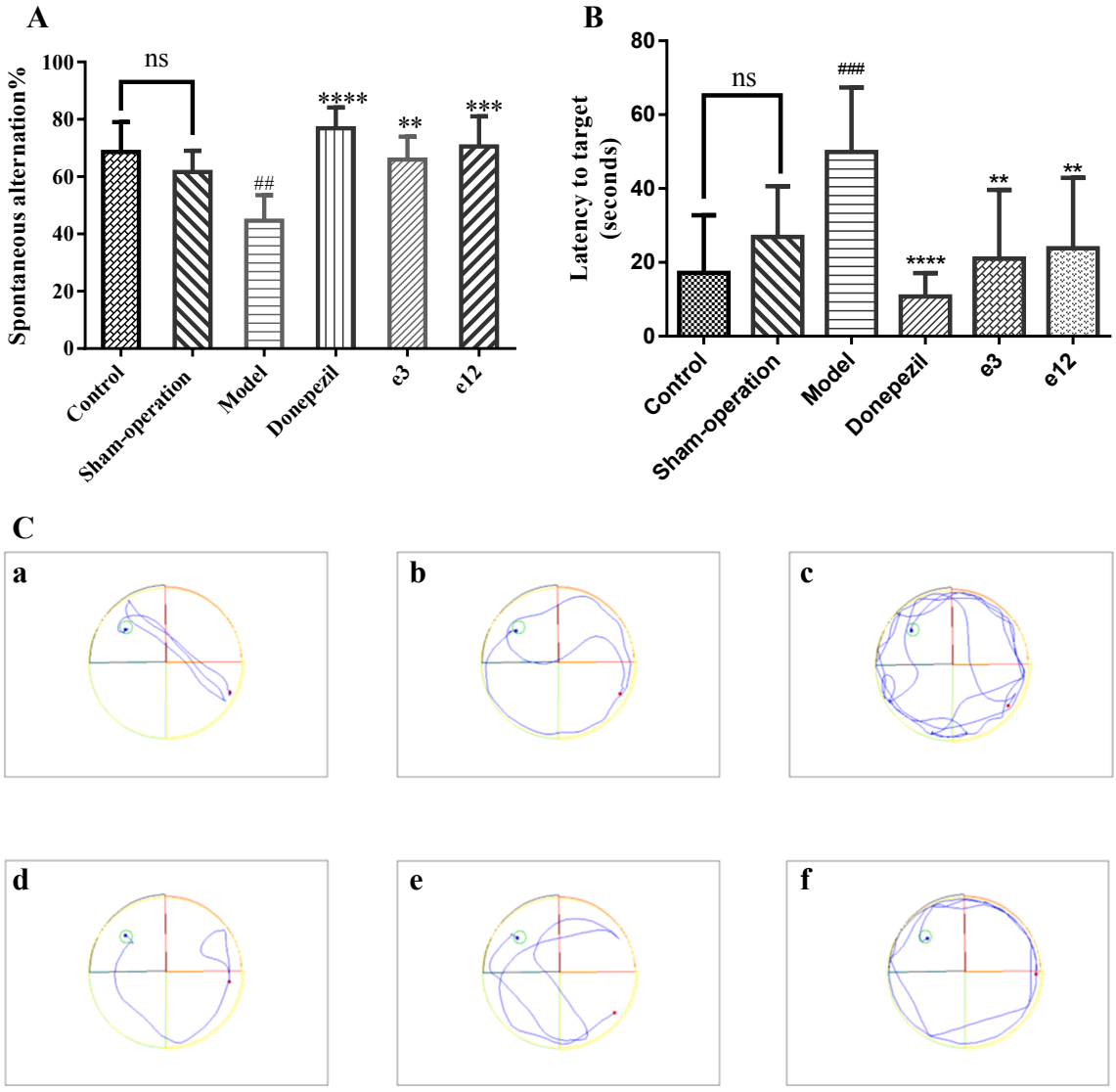

Fig. 9. Effects of oral administration of compounds **e3** and **e12** (15 mg/kg) on $A\beta_{1-42}$-induced induce acute neurotoxicity in ICR mice determined by the Y maze and Morris water maze test. Donepezil was used as a positive control. (A) Effect of the compounds on $A\beta_{1-42}$-induced spontaneous alternation deficits of mice in Y maze. (B) The escape latency values to target in Morris water maze. (C) The trajectories of mice in control (a), sham-operation (b), model (c), donepezil (d), **e3** (e), and **e12** (f) group in the Morris water maze test. Data are presented as the mean ± SEM (n = 6; $^{\#\#}p < 0.01$, $^{\#\#\#}p < 0.001$ vs. sham-operation; $^{**}p < 0.01$, $^{***}p < 0.001$, $^{****}p < 0.0001$vs. model.)

(1 equiv) and triethylamine (4 equiv) in dry tetrahydrofuran and stirred at room temperature for 12 h. When the substrates disappeared (as detected by TLC), saturated sodium bicarbonate was added to neutralize acid. The reaction mixture was extracted with CH_2Cl_2 for three times. The organic layer was dried over anhydrous sodium sulfate, evaporated to give the crude product, which was purified by silica column chromatography.

*4.1.3.1. 6-Methoxy-1-methyl-1,2,3,4-tetrahydro-β-carboline (**2a**).* Compound **2a** was prepared according to general procedure I.

Yellow solid, yield: 80%. ^{1}H NMR (300 MHz, DMSO-d_6) δ 11.19 (s, 1H), 7.47 (d, J = 7.8 Hz, 1H), 7.37 (d, J = 8.1 Hz, 1H), 7.17–7.08 (m, 1H), 7.07–6.97 (m, 1H), 4.06 (q, J = 6.5 Hz, 1H), 3.75 (s, 3H), 3.61 (dd, J = 11.7, 5.6 Hz, 2H), 2.93 (d, J = 5.3 Hz, 2H), 1.6 (d, J = 7.3 Hz,3H).

*4.1.3.2. 1-Methyl-1,2,3,4-tetrahydro-β-carboline (**2b**)*. Compound **2b** was prepared according to general procedure I. Yellow solid, yield: 80%. ^{1}H NMR (300 MHz, DMSO-d_6) δ 11.19 (s, 1H), 9.58 (s, 1H), 9.16 (s, 1H), 7.47 (d, J = 7.8 Hz, 1H), 7.37 (d, J = 8.1 Hz, 1H), 7.18–6.97 (m, 2H), 4.6 (q, J = 6.5 Hz, 1H), 3.61 (dd, J = 11.7, 5.6 Hz, 2H), 2.93 (d, J = 5.2 Hz, 2H), 1.65 (d, J = 7.4 Hz, 3H).

*4.1.3.3. (E)-3-(4-hydroxyphenyl)-1-(6-methoxy-1-methyl-1,3,4,9-tetrahydro-2H-pyrido[3,4-b]indol-2-yl)prop-2-en-1-one (**e1**)*. Compound **e1** was prepared according to general procedure III. White solid, yield: 87%. ^{1}H NMR (300 MHz, DMSO-d_6) δ 10.72 (d, J = 18.0 Hz, 1H), 9.88 (s, 1H), 7.82 (t, J = 10.4 Hz, 2H), 7.62–7.51 (m, 1H), 7.39 (dd, J = 15.9, 4.5 Hz, 1H), 7.33–7.11 (m, 4H), 6.93 (q, J = 2.6 Hz, 1H), 6.70 (dq, J = 8.7, 2.2 Hz, 1H), 5.67 (q, J = 6.4 Hz, 1H), 5.67 (d, J = 7.4 Hz, 1H), 3.74 (d, J = 6.9 Hz, 3H), 3.51–3.15 (m, 2H), 2.72–2.65 (m, 2H), 1.45 (d, J = 6.8 Hz, 3H). ^{13}C NMR (126 MHz, DMSO-d_6) δ 165.59, 159.43, 153.59, 142.59, 136.99, 131.40, 130.33, 129.69, 127.12, 126.71, 122.68, 116.07, 115.34, 112.10, 110.97, 106.61, 100.49, 55.81, 48.75, 45.71, 22.77, 19.39. MS(ESI) m/z Calcd for $C_{22}H_{22}N_2O_3$ [M + Na]$^+$: 385.43. Found: 385.33.

*4.1.3.4. (E)-3-(benzo[d][1,3]dioxol-5-yl)-1-(6-methoxy-1-methyl-1,3,4,9-tetrahydro-2H-pyrido[3,4-b]indol-2-yl)prop-2-en-1-one (**e2**)*. Compound **e2** was prepared according to general procedure III. Brown solid, yield: 82%. ^{1}H NMR (400 MHz, DMSO-d_6) δ 10.74 (s, 1H), 7.56 (d, J = 2.1 Hz, 1H), 7.53–7.44 (m, 2H), 7.30–7.12 (m, 4H), 6.99–6.89 (m, 2H), 6.70 (dt, J = 8.8, 2.0 Hz, 1H), 6.09 (s, 2H), 5.66 (q, J = 6.6 Hz, 1H), 3.76 (d, J = 1.6 Hz, 3H), 3.42 (dt, J = 14.6, 7.2 Hz, 1H), 3.18 (dd, J = 5.3, 1.8 Hz, 1H), 2.73 (d, J = 6.7 Hz, 2H), 1.45 (d, J = 6.6 Hz, 3H). ^{13}C NMR (100 MHz, DMSO-d_6) δ 165.40, 153.62, 149.03, 148.42, 142.28, 133.37, 133.24, 131.42, 127.13, 124.74, 117.05, 112.11, 110.98, 108.83, 107.06, 106.63, 101.88, 100.50, 55.82, 48.78, 45.77, 22.77, 19.38. MS(ESI) m/z Calcd for $C_{23}H_{22}N_2O_4$ [M + Na]$^+$: 413.44. Found: 413.24.

*4.1.3.5. (E)-3-(3,4-dihydroxyphenyl)-1-(6-methoxy-1-methyl-1,3,4,9-tetrahydro-2H-pyrido[3,4-b]indol-2-yl)prop-2-en-1-one (**e3**)*. Compound **e3** was prepared according to general procedure III. White solid, yield: 86%. ^{1}H NMR (500 MHz, DMSO-d_6) δ 10.92 (s, 1H), 9.47 (s, 1H), 9.03 (s, 1H), 7.44–7.36 (m, 2H), 7.32 (d, J = 8.4 Hz, 1H), 7.14 (d, J = 12.0 Hz, 1H), 7.09–7.01 (m, 3H), 6.98 (q, J = 7.3, 6.6 Hz, 1H), 6.77 (d, J = 8.1 Hz, 1H), 5.68 (q, J = 6.7 Hz, 1H), 4.47 (d, J = 14.0 Hz, 1H), 3.74 (d, J = 6.9 Hz, 3H), 3.48–3.41 (m, 1H), 2.76 (d, J = 7.6 Hz, 2H), 1.46 (d, J = 6.7 Hz, 3H). ^{13}C NMR (126 MHz, DMSO-d_6) δ 165.55, 153.59, 147.88, 145.90, 142.97, 137.02, 131.39, 127.20, 127.12, 121.21, 120.74, 116.07, 115.23, 112.10, 111.17, 106.60, 100.47, 55.81, 48.75, 46.17, 22.77, 19.40. MS(ESI) m/z Calcd for $C_{22}H_{22}N2O_4$ [M + Na]$^+$: 401.43. Found: 401.29.

*4.1.3.6. (E)-1-(6-methoxy-1-methyl-1,3,4,9-tetrahydro-2H-pyrido[3,4-b]indol-2-yl)-3-(3,4,5-trimethoxyphenyl)prop-2-en-1-one (**e4**)*. Compound **e4** was prepared according to general procedure III. Yellow solid, yield: 82%. ^{1}H NMR (400 MHz, DMSO-d_6) δ 10.78 (s, 1H), 7.55 (dd, J = 15.2, 6.5 Hz, 1H), 7.35 (d, J = 15.3 Hz, 1H), 7.23 (d, J = 8.7 Hz, 1H), 7.10 (d, J = 10.5 Hz, 2H), 6.93 (d, J = 2.5 Hz, 1H), 6.72 (dd, J = 8.7, 2.5 Hz, 1H), 5.77–5.70 (m, 1H), 4.49 (d, J = 15.2 Hz, 1H),3.86 (d, J = 4.9 Hz, 6H), 3.76 (s, 3H), 3.72 (s, 3H), 3.67–3.51 (m, 1H), 2.78 (d, J = 8.8 Hz, 2H), 1.49 (d, J = 6.8 Hz,3H). ^{13}C NMR (100 MHz, DMSO-d_6) δ 165.30, 153.64, 153.54, 153.54,142.73, 139.29, 136.95, 131.47, 131.31, 127.15, 118.33, 112.11, 110.98, 106.54, 106.15, 106.09, 100.53, 60.55, 56.52, 55.80, 55.33, 48.82, 45.76, 22.90, 19.40. MS(ESI) m/z Calcd for $C_{25}H_{28}N_2O_5$[M + H]$^+$: 437.51. Found: 437.22.

*4.1.3.7. 3-(3,4-Dihydroxyphenyl)-1-(6-methoxy-1-methyl-1,3,4,9-tetrahydro-2H-pyrido[3,4-b]indol-2-yl)propan-1-one (**e5**)*. Compound **e5** was prepared according to general procedure III. Yellow solid, yield: 88%. ^{1}H NMR (400 MHz, DMSO-d_6) δ 10.60 (s, 1H), 8.57 (d, J = 26.7 Hz, 2H), 7.09 (dd, J = 8.7, 6.4 Hz, 1H), 6.79 (dd, J = 4.5, 2.4 Hz, 1H), 6.63–6.47 (m, 3H), 6.39 (ddd, J = 7.2, 5.0, 2.1 Hz, 1H), 5.46 (q, J = 6.6 Hz, 1H), 3.64 (s, 3H), 3.26–3.09 (m, 2H), 2.65–2.49 (m, 6H), 1.27 (d, J = 6.7 Hz, 3H). ^{13}C NMR (75 MHz, DMSO-d_6) δ 170.80, 153.58, 145.44, 143.78, 137.00, 132.73, 131.50, 127.10, 119.37, 116.31, 115.86, 112.04, 110.92, 106.53, 100.45, 55.79, 48.49, 45.10, 35.52, 30.80, 21.21, 19.31. MS(ESI) m/z Calcd for $C_{22}H_{24}N_2O_4$ [M + Na]$^+$: 403.44. Found: 403.25.

*4.1.3.8. (E)-3-(3,4-dimethoxyphenyl)-1-(6-methoxy-1-methyl-1,3,4,9-tetrahydro-2H-pyrido[3,4-b]indol-2-yl)prop-2-en-1-one (**e6**)*. Compound **e6** was prepared according to general procedure III. Yellow solid, yield: 84%. ^{1}H NMR (300 MHz, DMSO-d_6) δ 10.76 (s, 1H), 7.93–7.51 (m, 2H), 7.24 (d, J = 24.0 Hz, 2H), 7.01–6.83 (m, 2H), 6.80–6.62 (m, 1H), 5.69 (q, J = 6.9 Hz, 1H), 4.48 (d, J = 13.8 Hz, 1H), 3.84 (d, J = 6.7 Hz, 6H), 3.76 (d, J = 5.3 Hz, 3H), 3.67–3.47 (m, 1H), 3.03–2.66 (m, 2H), 1.47 (d, J = 6.7 Hz, 3H). ^{13}C NMR (126 MHz, DMSO-d_6) δ 165.46, 155.17, 153.63, 152.68, 142.27, 137.01, 136.62, 131.43, 127.15, 123.22, 122.04, 117.64, 112.07, 110.96, 108.80, 106.56, 100.53, 56.43, 55.82, 55.34, 48.81, 45.77, 22.80, 19.40. MS (ESI) m/z Calcd for $C_{24}H_{26}N_2O_4$ [M + Na]$^+$: 429.48. Found: 429.24.

*4.1.3.9. (E)-3-(2,6-dimethoxyphenyl)-1-(6-methoxy-1-methyl-1,3,4,9-tetrahydro-2H-pyrido[3,4-b]indol-2-yl)prop-2-en-1-one (**e7**)*. Compound **e7** was prepared according to general procedure III. Yellow solid, yield: 88%. ^{1}H NMR (300 MHz, Chloroform-*d*) δ 8.80 (s, 1H), 8.03 (d, J = 15.6 Hz, 1H), 7.27 (d, J = 6.9 Hz, 1H), 7.17–7.03 (m, 2H), 6.99–6.86 (m, 3H), 6.83 (dd, J = 8.7, 2.5 Hz, 1H), 5.95 (q, J = 6.7 Hz, 1H), 4.42–4.27 (m, 1H), 3.88 (d, J = 2.9 Hz, 6H), 3.84 (s, 3H), 3.71–3.47 (m, 1H), 2.87 (td, J = 17.9, 16.9, 12.0 Hz, 2H), 1.58 (d, J = 6.7 Hz, 3H). ^{13}C NMR (75 MHz, Chloroform-*d*) δ 166.23, 153.99, 153.48, 152.66, 138.17, 136.33, 131.34, 127.02, 125.03, 118.96, 115.76, 112.38, 111.31, 106.91, 104.32, 104.04, 100.38, 56.15, 56.01, 55.89, 53.46, 46.19, 22.56, 19.27. MS(ESI) m/z Calcd for $C_{24}H_{26}N_2O_4$[$M - H$]$^-$ 405.48. Found: 405.21.

*4.1.3.10. (E)-1-(6-methoxy-1-methyl-1,3,4,9-tetrahydro-2H-pyrido[3,4-b]indol-2-yl)-3-(2,3,4-trimethoxyphenyl)prop-2-en-1-one (**e8**)*. Compound **a8** was prepared according to general procedure III. Yellow solid, yield: 88%. ^{1}H NMR (300 MHz, Chloroform-*d*) δ 8.60 (s, 1H), 7.91 (d, J = 15.5 Hz, 1H), 7.40–7.16 (m, 2H), 7.08 (d, J = 15.5 Hz, 1H), 6.94 (d, J = 2.4 Hz, 1H), 6.83 (dd, J = 8.7, 2.5 Hz, 1H), 6.73 (d, J = 8.8 Hz, 1H), 5.93 (q, J = 6.9 Hz, 1H), 4.33 (d, J = 13.9 Hz, 1H), 3.94 (d, J = 9.4 Hz, 9H), 3.87 (s, 3H), 3.66–3.47 (m, 1H), 3.03–2.66 (m, 2H), 1.58 (d, J = 6.7 Hz, 3H). ^{13}C NMR (75 MHz, Chloroform-*d*) δ 165.94, 154.96, 154.04, 153.10, 142.50, 138.20, 136.05, 131.96, 131.29, 127.05, 122.37, 117.18, 111.76, 111.34, 107.56, 107.07, 100.42, 61.24, 60.96, 56.08, 56.01, 53.44, 46.13, 22.58, 19.27. MS (ESI) m/z Calcd for $C_{25}H_{28}N_2O_5$ [M−H]$^-$: 435.51. Found: 435.25.

*4.1.3.11. (E)-1-(6-methoxy-1-methyl-1,3,4,9-tetrahydro-2H-pyrido[3,4-b]indol-2-yl)-3-(naphthalen-2-yl)prop-2-en-1-one (**e9**)*. Compound **e9** was prepared according to general procedure III. Yellow solid, yield: 88%. ^{1}H NMR (300 MHz, Chloroform-d) δ 9.01–8.75 (m, 1H), 8.63 (d, J = 15.2 Hz, 1H), 8.31–8.20 (m, 1H), 7.97–7.84 (m, 2H), 7.81 (d, J = 7.1 Hz, 1H), 7.56 (dtd, J = 10.6, 7.3, 3.1 Hz, 3H), 7.33 – 7.26 (m, 1H), 7.11 (d, J = 15.2 Hz, 1H), 6.97 (d, J = 2.5 Hz, 1H), 6.85 (dd, J = 8.7, 2.5 Hz, 1H), 6.00 (q, J = 6.7 Hz, 1H), 4.37 (dd, J = 14.0,

4.6 Hz, 1H), 3.89 (s, 3H), 3.72–3.51 (m, 1H), 3.06–2.73 (m, 2H), 1.63 (d, J = 6.8 Hz, 3H). ^{13}C NMR (100 MHz, DMSO-d_6) δ 165.11, 153.67, 138.46, 136.90, 133.78, 132.56, 131.47, 131.36, 130.16, 129.13, 127.38, 127.19, 126.62, 126.14, 125.52, 123.58, 122.12, 112.14, 111.04, 106.63, 100.54, 55.38, 48.95, 45.95, 22.82, 19.45. MS(ESI) m/z Calcd for $C_{26}H_{24}N_2O_2$ [M − H]$^-$: 395.49. Found: 395.25.

4.1.3.12. (E)-3-(4-hydroxyphenyl)-1-(1-methyl-1,3,4,9-tetrahydro-2H-pyrido[3,4-b]indol-2-yl)prop-2-en-1-one ***(e10)***. Compound **e10** was prepared according to general procedure III. White solid, yield: 85%. ^{1}H NMR (300 MHz, DMSO-d_6) δ 10.97 (s, 1H), 10.91 (s, 1H), 7.91 (d, J = 8.3 Hz, 2H), 7.58 (d, J = 15.4 Hz, 1H), 7.50–7.35 (m, 5H), 7.12–6.94 (m, 3H), 5.65 (q, J = 6.4 Hz, 1H), 3.41–3.25 (m, 2H),2.78 (t, J = 6.7 Hz, 2H), 1.48 (d, J = 6.8 Hz, 3H). ^{13}C NMR (126 MHz, DMSO-d_6) δ 164.99, 149.83, 140.61, 136.38, 136.07, 130.70, 126.87, 126.76, 121.74, 121.35, 120.29, 118.99, 118.19, 115.99, 111.51, 106.65, 47.68, 45.77, 22.73, 19.33. MS(ESI) m/z Calcd for $C_{21}H_{20}N_2O_2$ [M + H]$^+$: 333.40. Found: 333.25.

4.1.3.13. (E)-3-(benzo[d][1,3]dioxol-5-yl)-1-(1-methyl-1,3,4,9-tetrahydro-2H-pyrido[3,4-b] indol-2-yl)prop-2-en-1-one ***(e11)***. Compound **e11** was prepared according to general procedure III. Brown solid, yield: 80%. ^{1}H NMR (400 MHz, DMSO-d_6) δ 10.92 (s, 1H), 7.56 (d, J = 1.7 Hz, 1H), 7.51 (d, J = 4.1 Hz, 1H), 7.47 (s, 1H), 7.42 (d, J = 7.8 Hz, 1H), 7.33 (t, J = 7.7 Hz, 1H), 7.10–7.02 (m, 1H), 7.01–6.90 (m, 2H), 6.09 (s, 2H), 5.69 (q, J = 6.6 Hz, 1H), 4.54 (d, J = 13.8 Hz, 1H), 3.44 (dt, J = 14.5, 8.0 Hz, 1H), 2.76 (d, J = 6.9 Hz, 2H), 1.47 (d, J = 6.7 Hz, 3H). ^{13}C NMR (100 MHz, DMSO-d_6) δ 165.15, 149.03, 148.42, 142.27, 136.22, 134.58, 130.11, 126.79, 124.76, 121.34, 119.00, 118.22, 117.06, 111.50, 108.84, 107.06, 106.73, 101.88, 48.73, 45.70, 22.73, 19.34. MS(ESI) m/z Calcd for $C_{22}H_{20}N_2O_3$ [M + Na]$^+$: 383.41. Found: 383.32.

4.1.3.14. (E)-3-(3,4-dihydroxyphenyl)-1-(1-methyl-1,3,4,9-tetrahydro-2H-pyrido[3,4-b]indol-2-yl)prop-2-en-1-one ***(e12)***. Compound **e12** was prepared according to general procedure III. White solid, yield: 76%. ^{1}H NMR (500 MHz, DMSO-d_6) δ 10.92 (s, 1H), 9.47 (s, 1H), 9.03 (s, 1H), 7.44–7.36 (m, 2H), 7.32 (d, J = 8.4 Hz, 1H), 7.14 (d, J = 12.0 Hz, 1H), 7.09–7.01 (m, 3H), 6.98 (q, J = 7.3, 6.6 Hz, 1H), 6.77 (d, J = 8.1 Hz, 1H), 5.68 (q, J = 6.7 Hz, 1H), 4.47 (d, J = 14.0 Hz, 1H), 3.48–3.41 (m, 1H), 2.76 (d, J = 7.6 Hz, 2H), 1.46 (d, J = 6.7 Hz, 3H). ^{13}C NMR (126 MHz, DMSO-d_6) δ 165.53, 147.89, 145.92, 142.93, 136.36, 132.99, 127.24, 126.81, 121.29, 121.18, 118.95, 118.18, 116.08, 115.39, 115.32, 111.48, 106.72, 48.69, 45.62, 22.72, 19.37. MS(ESI) m/z Calcd for $C_{21}H_{20}N_2O_3$ [M + H]$^+$: 348.4. Found: 349.21.

4.1.3.15. (E)-1-(1-methyl-1,3,4,9-tetrahydro-2H-pyrido[3,4-b]indol-2-yl)-3-(3,4,5-trimethoxyphenyl)prop-2-en-1-one ***(e13)***. Compound **e13** was prepared according to general procedure III. Yellow solid, yield: 85%. ^{1}H NMR (400 MHz, DMSO-d_6) δ 10.74 (s, 1H), 7.51 (dd, J = 15.2, 1.9 Hz, 1H), 7.36 (d, J = 7.7 Hz, 1H), 7.29 (d, J = 8.0 Hz, 1H), 7.16 (d, J = 15.1 Hz, 1H), 7.08–6.98 (m, 1H), 6.99–6.89 (m, 3H), 5.76 (d, J = 7.0 Hz, 1H), 4.49 (d, J = 15.2 Hz, 1H), 3.77–3.73 (m, 3H), 3.49 (d, J = 13.4 Hz, 1H), 2.77 (d, J = 31.2 Hz, 2H), 1.50 (d, J = 7.7 Hz, 3H). ^{13}C NMR (75 MHz, DMSO-d_6) δ 165.31, 153.41, 153.41, 142.57, 139.24, 136.38, 136.05, 131.16, 126.69, 121.17, 118.87, 118.05, 117.94, 111.37, 106.47, 105.72, 105.72,60.54, 56.36, 56.36, 48.81, 45.78, 22.83, 19.28. MS(ESI) m/z Calcd for $C_{24}H_{26}N_2O_4$ [M + Na]$^+$: 429.48. Found: 429.29.

4.1.3.16. 3-(3,4-Dihydroxyphenyl)-1-(1-methyl-1,3,4,9-tetrahydro-2H-pyrido[3,4-b]indol-2-yl)propan-1-one ***(e14)***. Compound **e14** was prepared according to general procedure III. Yellow solid, yield: 88%. ^{1}H NMR (300 MHz, DMSO-d_6) δ 10.93 (s, 1H), 8.73 (s, 2H), 7.37 (ddd, J = 24.4, 7.9, 3.8 Hz, 2H), 7.03 (dt, J = 25.9, 7.3 Hz, 2H), 6.75–6.37 (m, 3H), 5.60 (q, J = 6.6 Hz, 1H), 4.09 (d, J = 13.8 Hz, 1H), 3.34 (d, J = 13.0 Hz, 1H), 2.82–2.62 (m, 6H), 1.41 (d, J = 6.7 Hz, 3H). ^{13}C NMR (126 MHz, DMSO-d_6) δ 170.76, 145.43, 143.77, 136.35, 135.76, 132.60, 126.75, 121.29, 119.41, 118.96, 118.14, 116.31, 115.88, 111.46, 106.66, 48.47, 45.08, 35.51, 30.81, 22.23, 19.27. MS(ESI) m/z Calcd for $C_{21}H_{22}N_2O_3$ [M + Na]$^+$: 373.42. Found: 373.20.

4.1.3.17. (E)-3-(3,4-dimethoxyphenyl)-1-(1-methyl-1,3,4,9-tetrahydro-2H-pyrido[3,4-b]indol-2-yl)prop-2-en-1-one ***(e15)***. Compound **e15** was prepared according to general procedure III. Yellow solid, yield: 78%. ^{1}H NMR (300 MHz, Chloroform-d) δ 9.07 (s, 1H), 7.77 (d, J = 15.3 Hz, 1H), 7.50 (d, J = 7.6 Hz, 1H), 7.37 (d, J = 7.9 Hz, 1H), 7.16 (dtt, J = 13.8, 6.5, 2.9 Hz, 4H), 6.90 (q, J = 15.5, 11.5 Hz, 2H), 5.98 (q, J = 6.7 Hz, 1H), 4.42–4.29 (m, 1H), 4.05–3.85 (m, 6H), 3.67–3.52 (m, 1H), 2.90 (q, J = 13.1, 12.5 Hz, 2H), 1.58 (d, J = 6.7 Hz, 3H). ^{13}C NMR (75 MHz, DMSO-d_6) δ 165.40, 150.72, 149.38, 142.66, 136.29, 131.61, 128.48, 126.79, 122.85, 121.30, 118.96, 118.21, 116.55, 111.96, 111.49, 110.94, 106.68, 56.19, 55.98, 48.73, 45.63, 22.82, 19.38. MS (ESI) m/z Calcd for $C_{23}H_{24}N_2O_3$ [M + Na]$^+$: 399.46. Found: 399.28.

4.1.3.18. (E)-3-(2,6-dimethoxyphenyl)-1-(1-methyl-1,3,4,9-tetrahydro-2H-pyrido[3,4-b]indol-2-yl)prop-2-en-1-one ***(e16)***. Compound **e16** was prepared according to general procedure III. Yellow solid, yield: 75%. ^{1}H NMR (300 MHz, Chloroform-d) δ 9.33 (s, 1H), 8.11 (d, J = 15.5 Hz, 1H), 7.51 (d, J = 7.5 Hz, 1H), 7.42 (d, J = 7.8 Hz, 1H), 7.20–7.11 (m, 4H), 6.92 (h, J = 8.4, 7.9 Hz, 2H), 6.03 (q, J = 6.7 Hz, 1H), 4.50–4.16 (m, 1H), 3.88 (d, J = 10.9 Hz, 6H), 3.60 (td, J = 13.8, 5.0 Hz, 1H), 3.03–2.79 (m, 2H), 1.62 (d, J = 6.7 Hz, 3H). ^{13}C NMR (75 MHz, DMSO-d_6) δ 165.38, 153.69, 152.28, 136.63, 136.21, 134.00, 131.77, 126.80, 124.68, 121.30, 119.30, 118.96, 118.18, 116.74, 113.18, 111.49, 106.67, 56.49, 56.06, 48.78, 45.72, 22.79, 19.34. MS(ESI) m/z Calcd for $C_{23}H_{24}N_2O_3$ [M + H]$^+$: 377.46. Found: 377.35.

4.1.3.19. (E)-1-(1-methyl-1,3,4,9-tetrahydro-2H-pyrido[3,4-b]indol-2-yl)-3-(2,3,4-trimethoxyphenyl)prop-2-en-1-one ***(e17)***. Compound **e17** was prepared according to general procedure III. Yellow solid, yield: 84%. ^{1}H NMR (300 MHz, Chloroform-d) δ 9.42 (s, 1H), 8.02 (d, J = 15.5 Hz, 1H), 7.51 (d, J = 7.6 Hz, 1H), 7.38 (dd, J = 17.0, 8.2 Hz, 2H), 7.23–7.07 (m, 4H), 6.75 (d, J = 8.8 Hz, 1H), 6.04 (q, J = 6.7 Hz, 1H), 4.37 (dd, J = 13.0, 4.2 Hz, 1H), 3.98 (s, 3H), 3.95 (d, J = 5.3 Hz, 6H), 3.62 (ddd, J = 18.6, 10.8, 5.1 Hz, 1H), 2.93 (dd, J = 13.8, 12.5 Hz, 2H), 1.62 (d, J = 6.7 Hz, 3H). ^{13}C NMR (126 MHz, DMSO-d_6) δ 165.45, 155.17, 152.69, 142.27, 136.59, 136.36, 136.29, 126.80, 123.22, 122.03, 121.30, 118.96, 118.18, 117.65, 111.49, 108.83, 106.68, 61.78, 60.91, 56.47, 48.74, 45.69, 22.73, 19.36. MS(ESI) m/z Calcd for $C_{24}H_{26}N_2O_4$ [M + Na]$^+$: 429.48. Found: 429.29.

4.1.3.20. (E)-1-(1-methyl-1,3,4,9-tetrahydro-2H-pyrido[3,4-b]indol-2-yl)-3-(naphthalen-2-yl)prop-2-en-1-one ***(e18)***. Compound **e18** was prepared according to general procedure III. Yellow solid, yield: 88%. ^{1}H NMR (300 MHz, Chloroform-d) δ 8.59 (d, J = 15.2 Hz, 1H), 8.42 (s, 1H), 8.26 (d, J = 8.0 Hz, 1H), 7.92 (d, J = 8.0 Hz, 2H), 7.78 (t, J = 9.5 Hz, 1H), 7.55 (dq, J = 12.3, 6.5 Hz, 4H), 7.39 (d, J = 7.8 Hz, 1H), 7.25–7.03 (m, 2H), 5.99 (d, J = 6.9 Hz, 1H), 4.54 – 4.27 (m, 1H), 3.79–3.48 (m, 1H), 3.06–2.80 (m, 2H), 1.65 (t, J = 8.0 Hz, 3H). ^{13}C NMR (75 MHz, DMSO-d_6) δ 165.08, 153.65, 138.45, 136.15, 133.76, 132.53, 131.35, 130.15, 129.11, 127.35, 127.18, 126.60, 126.13, 125.49, 123.56, 122.08, 121.45, 118.99, 118.21, 111.52, 106.61, 48.85, 45.95, 22.74, 19.40. MS(ESI) m/z Calcd for $C_{25}H_{22}N_2O$ [M + Na]$^+$: 389.46. Found: 389.25.

4.2. Biological assays

4.2.1. ThT assay [66]

Aβ_{1-42}(Beyotime) was dissolved in HFIP to give a stock solution (1 mg/mL), which was aliquoted into small samples and stored at − 80 °C after solvent was evaporated. Solutions of test compounds were prepared in DMSO at 30 mM for storage. For the inhibition of self-

induced $A\beta_{1-42}$ aggregation experiment, the pretreated $A\beta_{1-42}$ and compounds were diluted with 50 mM phosphate buffer (pH 7.4) to 50 μM before use. A mixture of the peptide (20 μL, 25 μM, final concentration) with or without the tested compound (20 μL, 20 μM, final concentration) was incubated at 37 °C for 24 h and used 50 mM phosphate buffer (pH 7.4) instead of Aβ as a blank. After incubation, 160 μL of 50 mM glycine-NaOH buffer (pH 8.0) containing thioflavin T (5 μM) was added. Fluorescence was measured on a Varioskan Flash Multimode Reader (excitation, 450 nm; emission, 485 nm). The percent inhibition of aggregation was calculated by the expression (1–IFi/IFc) × 100, where IFi and IFc were the fluorescence intensities obtained for Aβ in the presence and absence of inhibitors after subtracting the background, respectively.

4.2.2. Cholinesterase inhibition assay in vitro [67]

AChE (E.C.3.1.1.7, Type VI-S, from Electric Eel), BuChE (E.C.3.1.1.8, Type VI-S, from equine serum), 5,5′-dithiobis-2-nitrobenzoic acid (Ellman's reagent, DTNB), acetylthiocholine chloride (ATC), and butyrylthiocholine chloride (BTC) were purchased form Sigma Aldrich (Steinheim, Germany). Enzyme solutions were prepared to give 2.5 units ml^{-1} in 1.4 mL aliquots. Solutions of test compounds were prepared in DMSO at 30 mM and diluted in methanol to different concentrations ($10^{-3}-10^{-9}$ M) before use. The assay buffer was prepared from 13.6 g of potassium dihydrogen phosphate (100 mmol), which was dissolved in 1L of water and adjusted with KOH to pH = 7.9–8.1. Furthermore, 0.01 M DTNB solution, 0.075 M ATC and BTC solutions were prepared with assay buffer (pH 8.0).

In 96-well plates, 40 μL of phosphate buffer, 10 μL of the test compounds and 10 μL of enzyme, were added in turn and incubated for 2 min, followed by the addition of 0.01 M DTNB (20 μL) solution and substrate (20 μL). Activity was determined by measuring the absorbance at 405 nm at 37 °C, each concentration in triplicate. Blanks containing all components except enzyme were carried out. The concentration of compound producing 50% of enzyme activity inhibition (IC50) was calculated by nonlinear regression analysis of the response-concentration (log) curve, using the Graph-Pad Prism program package.

The *in vitro* BuChE assay (BuChE or BTC as the enzyme substrate) was conducted using a method similar to that described above.

4.2.3. In vitro activity

4.2.3.1. Cell culture. Rat pheochromocytoma PC12 cells, murine BV-2 microglial cells, Human SH-SY5Y neuroblastoma cells, hippocampal neuronal HT22 cell and human L02 hepatocytes were obtained from the Cell Bank of the Chinese Academy of Sciences (Shanghai, China). PC12, SH-SY5Y and BV-2 cells were maintained in Dulbecco's modified Eagle medium (DMEM) supplemented with 10% fetal bovine serum, 100 U/mL penicillin, and 100 μg/mL streptomycin at 37 °C under 5% CO_2.

4.2.3.2. Cell treatment. For cytotoxicity experiments, PC12, BV-2, SH-SY5Y, HT22 and L02 cells were seeded in 96-well plates at a density of 10^4 cells per well and treated with synthetic compounds except for blanks. For neuroprotective cell experiment [68], PC12 and SH-SY5Y cells were subcultured in 96-well plates at a seeding density of 10^4 cells per well and treated with modeling agent (H_2O_2, OA, $A\beta_{1-42}$) in the absence (control) or in the presence of compounds.

4.2.3.3. Cell viability assay. Cell viability was analyzed with 3-[4,5-dimethylthylthiazol-2,5-diphenyl-tetrazolium bromide] (MTT) assay method [69]. After incubation, the MTT reagent (15 μL/well) was added to each well and incubated for additional 4 h followed by solubilization of formazan crystals in DMSO (100 μL/well). The absorbance of each well was measured at a wavelength of 492 nm by a 1500 microplate reader (Thermo Fisher Scientific Co.). Results are expressed as the mean ± SEM of three independent experiments.

4.2.3.4. Measurement of intracellular ROS [70]. Briefly, 10^4 cells were seeded in a 96-well plate and treated with 2.5 μM or 5 μM of compounds and then incubated at 37 °C with 2.5 mg/ml of LPS for 24 h to induce ROS production. Then 2′,7′-dichlorodihydro fluorescein diacetate (DCFH-DA) (15 μM) was added for 30 min at 37 °C and media was then removed, cells were washed with DMEM for three times. The fluorescence distribution was observed and photographed by inverted fluorescence microscope and the fluorescence intensity was quantified by Image J software.

4.2.4. Molecular docking study

The crystal structures of amyloid forming peptide KLVFFA (PDB ID: 3OVJ) and hBChE (PDB ID: 4TPK) were derived from the RCSB Protein Data Bank (PDB). Docking studies were carried out using the discovery studio (DS, version 3.0, BIOVIA, San Diego, CA) for compound **e12**. Two protein structures were preprocessed by "prepare protein" module in DS to give the structures suitable for docking. "Prepare ligands" module in DS was applied for the structural preparation of the test compounds. The native ligand in the crystal structure was used to define the binding site. The binding site was defined as a site sphere (in 10 Å radius) around the original ligands in the co-crystal structures. The docking program CDOCKER encoded in DS 2019 was applied to identify the potential binding pattern of compound **e12** to the amyloid forming peptide KLVFFA and the hBChE. Other CDOCKER parameters were set as default.

4.2.4.1. Predicted physicochemical properties. The ADMET properties and physicochemical properties of compounds presented in this study were calculated using QikProp and Discovery Studio 2019.

4.2.5. In vivo activity [71]

Protocols for the behavioral experiments were established previously. Briefly, the adult male ICR mice (8–10 weeks old, weight 20–25 g) were obtained from the Qinglongshan animal breeding factory (Nanjing, China, NO.201930647). All animal handling and experimental protocols were approved by the Institutional Animal Care and Use Committee of the China Pharmaceutical University. Amyloid β peptide (1–42) was purchased from Beyotime. Donepezil that was gained from Energy Chemical (Shanghai, China) was used as the positive control.

4.2.5.1. Pretreatment of $A\beta_{1-42}$ and compounds. A stock solution of $A\beta_{1-42}$ was prepared by dissolving powdered Aβ peptide in saline to a final concentration of 2 μg/μL. The stock solution incubated at 37 °C for 7 days to induce aggregation. Compounds were weighed, dissolved in pure DMSO at a concentration of 150 mg/mL, and diluted by 100-fold with saline to final test concentrations.

4.2.5.2. Hippocampal injection and administration [72]. The mice were anesthetized with 2% Pentobarbital Sodium, fixed on the stereotaxic apparatus (Narishige, Japan), cut off the top skin of the head, wiped with alcohol cotton, and exposed the bregma and sagittal suture. The right hippocampus was located in 1.5 mm behind the bregma to the posterior and 2 mm to the right the sagittal suture. A small hole was punctured at this position, the depth of which was 2 mm below the skull surface. Each mouse was injected 5 μL $A\beta_{1-42}$ (2 μg/μL) at a constant rate of 2.5 μL/min. In the sham operated group, 5 μL saline was injected instead of $A\beta_{1-42}$. Three days after the operation, each group was given drug treatment. Donepezil and the synthesized compounds were orally administered (15 mmol/kg body weight) to mice and the control group was given normal saline. Two weeks after administration, the cognitive function of the mice was evaluated.

4.2.5.3. Morris water maze test [73]. The water maze system consists of a black pool (120 cm diameter, 60 cm height) with a depth of 40 cm water, escape platform (10 cm diameter, at the center of pool) camera system and an Xeye animal behavior analysis system.

4.2.5.4. Acquired training. The mice were put into the water from the opposite quadrant of the platform, with their heads facing the pool wall. The time for the mouse to find the platform (a successful escape) was recorded. If a mouse failed to reach the platform within 90 s, the test was terminated and the animal was gently navigated to the platform by hand. It was kept on the platform for 10 s. Each animal was trained 4 times a day with a 15–20 min interval between the two training sessions for 6 consecutive days.

4.2.5.5. Exploration training. On the second day after the last acquisition training, the platform was removed and exploration training was conducted. Animals were placed in the water from the opposite of the original platform quadrant. Record the time spent by the animal in the target quadrant (the quadrant where the platform was originally placed) and the number of times it entered the quadrant, which was used as a detection indicator of spatial memory.

4.2.5.6. Spontaneous Alternation Performances in Y Maze [74]. After the water maze test, all animals were tested for spontaneous alternation performance in the Y maze to evaluate their spatial working memory. The Y maze is made of blue poly. Each arm is 40 cm long, 13 cm high, 10 cm wide, and converging at an equal angle. Each mouse was placed at the end of one arm and allowed to explore the maze freely for 5 min. The sequence of arm entries (including possible returns into the same arm) was checked visually and noted down. If the mouse enters all three arms on consecutive occasion, this is defined as an alternation. Therefore, the total number of arm entries minus two is also the maximum number of alternations. The percentage of alternation was calculated as (actual alternations/maximum alternations) × 100. Parameters for the evaluation of behavior are given as the percentage of alternation (memory index) and the total number of arm entries (exploration index).

4.2.5.7. Acute Toxicity [75]. The adult male ICR mice (8–10 weeks old, weight 20–25 g) obtained from the Qinglongshan animal breeding factory (Nanjing, China, NO.201930647) were used to evaluate the acute toxicity of compounds **e3** and **e12**. Compounds was suspended in PEG-400 and normal saline at concentrations of 200 $mgmL^{-1}$ and given via oral administration according to the divided experimental groups (200 mg/kg,600 mg/kg, n = 5). After the administration of the compounds, the mice were observed continuously for the first 4 h for any abnormal behavior and mortality changes, intermittently for the next 24 h, and occasionally thereafter for 14 days for the onset of any delayed effects. All animals were sacrificed on the 14th day after drug administration and were macroscopically examined for possible damage to the heart, liver and kidneys.

4.2.5.8. Statistical analysis. Statistical analysis was carried out by one-way analysis of variance (ANOVA) using Graphpad Prism 6.0 software. Results are expressed as the mean ± SEM of three independent experiments. A p value < 0.05 were considered significant.

Declaration of Competing Interest

The authors declared that there is no conflict of interest.

Acknowledgments

This work was financially supported by the Natural Science Foundation of China (Grant no. 81973207), “Double First-Class” University project (no. CPU2018GY34), and Fundamental Research Funds for the Central Universities (2015ZD010).

Appendix A. Supplementary material

Supplementary data to this article can be found online at https://doi.org/10.1016/j.bioorg.2020.103844.

References

[1] V.H. Finder, Alzheimer's disease: a general introduction and pathomechanism, J. Alzheimer's Dis.: JAD 22 (Suppl 3) (2010) 5–19.
[2] World Alzheimer Report, 2018. https://www.alz.co.uk/research/world-report-2018 (September 2018).
[3] G. Pepeu, M.G. Giovannini, Cholinesterase Inhibitors and Beyond, Curr Alzheimer Res 6 (2) (2009) 86–96.
[4] A. Rampa, M. Bartolini, A. Bisi, F. Belluti, S. Gobbi, V. Andrisano, A. Ligresti, V. Di Marzo, The first dual ChE/FAAH Inhibitors: new perspectives for Alzheimer's disease? ACS Med. Chem. Lett. 3 (3) (2012) 182–186.
[5] G. Pepeu, M.G. Giovannini, Cholinesterase inhibitors and memory, Chem. Biol. Interact. 187 (1–3) (2010) 403–408.
[6] M. Haupt, Alzheimer's disease: etiology, clinical aspects and therapy, Krankenpflege J. 30 (9) (1992) 393–398.
[7] D.A. Drachman, C.F. Lippa, The etiology of Alzheimer's disease: the pathogenesis of dementia. The role of neurotoxins, Ann. N. Y. Acad. Sci. 648 (1992) 176–186.
[8] B.J. Balin, A.P. Hudson, Etiology and pathogenesis of late-onset Alzheimer's disease, Curr. Allergy Asthma Rep. 14 (3) (2014) 417.
[9] J. Hardy, The amyloid hypothesis for Alzheimer's disease: a critical reappraisal, J. Neurochem. 110 (4) (2009) 1129–1134.
[10] V. Ramberg, Neuroinflammation in Alzheimer's Disease: Focus on NF-κB and C/EBP Transcription Factors, Department of Neurochemistry, Stockholm University, 2011.
[11] F. Zhang, L. Jiang, Neuroinflammation in Alzheimer's disease, Neuropsychiatr. Dis. Treat. 14 (4) (2015) 243–256.
[12] Y. Madav, S. Wairkar, B. Prabhakar, Recent therapeutic strategies targeting beta amyloid and tauopathies in Alzheimer's disease, Brain Res. Bull. 146 (2019) 171–184.
[13] C. Berk, M.N. Sabbagh, Successes and failures for drugs in latestage development for Alzheimer’s disease, Drugs Aging 30 (2013) 783–792.
[14] B. De Strooper, Lessons from a failed gamma-secretase Alzheimer trial, Cell 159 (2014) 721–726.
[15] Y.J. Yu, R.J. Watts, Developing therapeutic antibodies for neurodegenerative disease, Neurotherapeutics 10 (2013) 459–472.
[16] Won H. Suh, Kenneth S. Suslick, Yoo-Hun Suh, Therapeutic agents for Alzheimers disease, Curr. Alzheimer Res. 5 (4) (2005).
[17] D. Muñoz-Torrero, Acetylcholinesterase inhibitors as disease-modifying therapies for Alzheimer’s disease, Curr. Med. Chem. 15 (2008) 2433–2455.
[18] Q. Li, H. Yang, Y. Chen, H. Sun, Recent progress in the identification of selective butyrylcholinesterase inhibitors for Alzheimer's disease, Eur. J. Med. Chem. 132 (2017) 294–309.
[19] S. Butini, M. Brindisi, S. Brogi, S. Maramai, E. Guarino, A. Panico, A. Saxena, V. Chauhan, R. Colombo, L. Verga, E. De Lorenzi, M. Bartolini, V. Andrisano, E. Novellino, G. Campiani, S. Gemma, Multifunctional cholinesterase and amyloid beta fibrillization modulators. Synthesis and biological investigation, ACS Med. Chem. Lett. 4 (12) (2013) 1178–1182.
[20] A. Mullard, Alzheimer amyloid hypothesis lives on, Nat. Rev. Drug Discovery 16 (2016) 3–5.
[21] J.T. Zhou, X.Y. Jiang, S.Y. He, H.L. Jiang, F. Feng, W.Y. Liu, W. Qu, H.P. Sun, Rational design of multitarget-directed ligands: strategies and emerging paradigms, J. Med. Chem. 62 (20) (2019) 8881–8914.
[22] Z.R. Wang, J.H. Hu, X.P. Yang, X. Feng, X.S. Li, L. Huang, A.S.C. Chan, Design, synthesis, and evaluation of orally bioavailable quinoline-indole derivatives as innovative multitarget-directed ligands: promotion of cell proliferation in the adult murine hippocampus for the treatment of Alzheimer's disease, J. Med. Chem. 61 (5) (2018) 1871–1894.
[23] X.M. Zha, D. Lamba, L.L. Zhang, Y.H. Lou, C.X. Xu, D. Kang, L. Chen, Y.G. Xu, L.Y. Zhang, A. De Simone, S. Samez, A. Pesaresi, J. Stojan, M.G. Lopez, J. Egea, V. Andrisano, M. Bartolini, Novel tacrine-benzofuran hybrids as potent multitarget-directed ligands for the treatment of Alzheimer's disease: design, synthesis, biological evaluation, and X-ray crystallography, J. Med. Chem. 59 (1) (2016) 114–131.
[24] S.S. Bharate, S. Mignani, R.A. Vishwakarma, Why are the majority of active compounds in the CNS domain natural products? A critical analysis, J. Med. Chem. 61 (23) (2018) 10345–10374.
[25] A. Al-Shamma, S. Drake, D.L. Flynn, L.A. Mitscher, Y.H. Park, G.S. Rao, A. Simpson, J.K. Swayze, T. Veysoglu, S.T. Wu, Antimicrobial agents from higher plants. Antimicrobial agents from Peganum harmala seeds, J. Nat. Prod. 44 (6) (1981) 745–747.
[26] M.M. Airaksinen, I. Kari, Beta-carbolines, psychoactive compounds in the mammalian body. Part I: Occurrence, origin and metabolism, Med. Biol. 59 (1) (1981) 21–34.
[27] M.M. Airaksinen, I. Kari, beta-Carbolines, psychoactive compounds in the mammalian body. Part II: Effects, Med. Biol. 59 (4) (1981) 190–211.
[28] J. Dai, W. Dan, U. Schneider, J. Wang, beta-Carboline alkaloid monomers and dimers: Occurrence, structural diversity, and biological activities, Eur. J. Med. Chem. 157 (2018) 622–656.
[29] K.M. Brummond, J.R. Goodell, M.G. Laporte, L. Wang, X.Q. Xie, Synthesis and in silico screening of a library of beta-carboline-containing compounds, Beilstein J. Org. Chem. 8 (2012) 1048–1058.

[30] Y. Schott, M. Decker, H. Rommelspacher, J. Lehmann, 6-Hydroxy- and 6-methoxy-beta-carbolines as acetyl- and butyrylcholinesterase inhibitors, Bioorg. Med. Chem. Lett. 16 (22) (2006) 5840–5843.
[31] R. Francik, G. Kazek, M. Cegla, M. Stepniewski, Antioxidant activity of beta-carboline derivatives, Acta Pol. Pharm. 68 (2) (2011) 185–189.
[32] J.R. Sanchez-Ramos, Banisterine and Parkinson's disease, Clin. Neuropharmacol. 14 (5) (1991) 391–402.
[33] M. Gruss, D. Appenroth, A. Flubacher, C. Enzensperger, J. Bock, C. Fleck, G. Gille, K. Braun, 9-Methyl-beta-carboline-induced cognitive enhancement is associated with elevated hippocampal dopamine levels and dendritic and synaptic proliferation, J. Neurochem. 121 (6) (2012) 924–931.
[34] J. Hamann, C. Wernicke, J. Lehmann, H. Reichmann, H. Rommelspacher, G. Gille, 9-Methyl-beta-carboline up-regulates the appearance of differentiated dopaminergic neurones in primary mesencephalic culture, Neurochem. Int. 52 (4–5) (2008) 688–700.
[35] W. Horton, A. Sood, S. Peerannawar, N. Kugyela, A. Kulkarni, R. Tulsan, C.D. Tran, J. Soule, H. LeVine 3rd, B. Torok, M. Torok, Synthesis and application of beta-carbolines as novel multi-functional anti-Alzheimer's disease agents, Bioorg. Med. Chem. Lett. 27 (2) (2017) 232–236.
[36] Y. Rook, K.U. Schmidtke, F. Gaube, D. Schepmann, B. Wunsch, J. Heilmann, J. Lehmann, T. Winckler, Bivalent beta-carbolines as potential multitarget anti-Alzheimer agents, J. Med. Chem. 53 (9) (2010) 3611–3617.
[37] R. Otto, R. Penzis, F. Gaube, O. Adolph, K.J. Fohr, P. Warncke, D. Robaa, D. Appenroth, C. Fleck, C. Enzensperger, J. Lehmann, T. Winckler, Evaluation of homobivalent carbolines as designed multiple ligands for the treatment of neurodegenerative disorders, J. Med. Chem. 58 (16) (2015) 6710–6715.
[38] Y. Zhao, F. Ye, J. Xu, Q. Liao, L. Chen, W. Zhang, H. Sun, W. Liu, F. Feng, W. Qu, Design, synthesis and evaluation of novel bivalent beta-carboline derivatives as multifunctional agents for the treatment of Alzheimer's disease, Bioorg. Med. Chem. 26 (13) (2018) 3812–3824.
[39] Z. Zhao, H. Song, J. Xie, T. Liu, X. Zhao, X. Chen, X. He, S. Wu, Y. Zhang, X. Zheng, Research progress in the biological activities of 3,4,5-trimethoxycinnamic acid (TMCA) derivatives, Eur. J. Med. Chem. 173 (2019) 213–227.
[40] A. Gaspar, E.M. Garrido, M. Esteves, E. Quezada, N. Milhazes, J. Garrido, F. Borges, New insights into the antioxidant activity of hydroxycinnamic acids: Synthesis and physicochemical characterization of novel halogenated derivatives, Eur. J. Med. Chem. 44 (5) (2009) 2092–2099.
[41] X. Zhang, X.X. He, Q.H. Chen, J.F. Lu, S. Rapposelli, R.B. Pi, A review on the hybrids of hydroxycinnamic acid as multi-target-directed ligands against Alzheimer's disease, Bioorg. Med. Chem. 26 (3) (2018) 543–550.
[42] W.X. Zhang, H. Wang, H.R. Cui, W.B. Guo, F. Zhou, D.S. Cai, B. Xu, X.H. Jia, X.M. Huang, Y.Q. Yang, H.S. Chen, J.C. Qi, P.L. Wang, H.M. Lei, Design, synthesis and biological evaluation of cinnamic acid derivatives with synergetic neuroprotection and angiogenesis effect, Eur. J. Med. Chem. 183 (2019) 111695.
[43] A.E. Roher, J.D. Lowenson, S. Clarke, A.S. Woods, R.J. Cotter, E. Gowing, M.J. Ball, beta-Amyloid-(1–42) is a major component of cerebrovascular amyloid deposits: implications for the pathology of Alzheimer disease, PNAS 90 (22) (1993) 10836–10840.
[44] S. Varadarajan, J. Kanski, M. Aksenova, C. Lauderback, D.A. Butterfield, Different mechanisms of oxidative stress and neurotoxicity for Alzheimer's A beta(1–42) and A beta(25–35), J. Am. Chem. Soc. 123 (24) (2001) 5625–5631.
[45] M. Rosini, E. Simoni, M. Bartolini, A. Cavalli, L. Ceccarini, N. Pascu, D.W. McClymont, A. Tarozzi, M.L. Bolognesi, A. Minarini, V. Tumiatti, V. Andrisano, I.R. Mellor, C. Melchiorre, Inhibition of acetylcholinesterase, beta-amyloid aggregation, and NMDA receptors in Alzheimer's disease: a promising direction for the multi-target-directed ligands gold rush, J. Med. Chem. 51 (15) (2008) 4381–4384.
[46] C. Lu, Y. Guo, J. Yan, Z. Luo, H.B. Luo, M. Yan, L. Huang, X. Li, Design, synthesis, and evaluation of multitarget-directed resveratrol derivatives for the treatment of Alzheimer's disease, J. Med. Chem. 56 (14) (2013) 5843–5859.
[47] R.M. Lataro, M.A.B. Silva, F.L. Mestriner, S.B.A. Cau, R.C.A. Tostes, H.C. Salgado, Chronic treatment with acetylcholinesterase inhibitors attenuates vascular dysfunction in spontaneously hypertensive rats, Am. J. Hypertens. 32 (6) (2019) 579–587.
[48] R. Shao, J. Xiao, Natural products for treatment of Alzheimer's disease and related diseases: understanding their mechanism of action, Curr. Neuropharmacol. 11 (2013) 337.
[49] M. Hoffmann, C. Stiller, E. Endres, M. Scheiner, S. Gunesch, C. Sotriffer, T. Maurice, M. Decker, Highly Selective butyrylcholinesterase inhibitors with tunable duration of action by chemical modification of transferable carbamate units exhibit pronounced neuroprotective effect in an Alzheimer's disease mouse model, J. Med. Chem. 62 (20) (2019) 9116–9140.
[50] C. Zheng, M. Zhou, J. Sun, H. Xiong, P. Peng, Z. Gu, Y. Deng, The protective effects of liraglutide on AD-like neurodegeneration induced by oxidative stress in human neuroblastoma SH-SY5Y cells, Chem. Biol. Interact. 310 (2019) 108688.
[51] M. Zhang, D. Wang, B. Li, Neuroprotection of two C21 steroidal glycosides from Cynanchum auriculatum against H2O2-induced damage on PC12 cells, Nat. Prod. Res. (2019) 1–4.
[52] E.W.L. Chan, S. Krishnansamy, C. Wong, S.Y. Gan, The NLRP3 inflammasome is involved in the neuroprotective mechanism of neural stem cells against microglia-mediated toxicity in SH-SY5Y cells via the attenuation of tau hyperphosphorylation and amyloidogenesis, Neurotoxicology 70 (2019) 91–98.
[53] D.D. Yan, J.L. Yao, Y. Liu, X. Zhang, Y.Q. Wang, X.Y. Chen, L.G. Liu, N. Shi, H. Yan, Tau hyperphosphorylation and P-CREB reduction are involved in acrylamide-induced spatial memory impairment: Suppression by curcumin, Brain Behav. Immun. 71 (2018) 66–80.
[54] M. Boban, M. Babic Leko, T. Miskic, P.R. Hof, G. Simic, Human neuroblastoma SH-SY5Y cells treated with okadaic acid express phosphorylated high molecular weight tau-immunoreactive protein species, J. Neurosci. Methods 319 (2019) 60–68.
[55] C.S. Kuruva, P.H. Reddy, Amyloid beta modulators and neuroprotection in Alzheimer's disease: a critical appraisal, Drug Discovery Today 22 (2) (2017) 223–233.
[56] Y. Zhu, X. Sun, T. Gong, Q. He, Z. Zhang, Antioxidant and antiapoptotic effects of 1,1'-(biphenyl-4,4'-diyl)-bis(3-(dimethylamino)-propan-1-one) on protecting PC12 cells from Abeta-induced injury, Mol. Pharm. 11 (2) (2014) 428–435.
[57] I. Morales, L. Guzman-Martinez, C. Cerda-Troncoso, G.A. Farias, R.B. Maccioni, Neuroinflammation in the pathogenesis of Alzheimer's disease. A rational framework for the search of novel therapeutic approaches, Front. Cell. Neurosci. (2014) 8.
[58] V. Calsolaro, P. Edison, Neuroinflammation in Alzheimer's disease: Current evidence and future directions, Alzheimer's Dementia: J. Alzheimer's Assoc. 12 (6) (2016) 719–732.
[59] S.K. Ravi, R.B. Narasingappa, M. Prasad, M.R. Javagal, B. Vincent, Cassia tora prevents Abeta1-42 aggregation, inhibits acetylcholinesterase activity and protects against Abeta1-42-induced cell death and oxidative stress in human neuroblastoma cells, Pharmacol. Rep.: PR 71 (6) (2019) 1151–1159.
[60] Y. Wang, C.S. Zhao, Sigma-1 receptor activation ameliorates LPS-induced NO production and ROS formation through the Nrf2/HO-1 signaling pathway in cultured astrocytes, Neurosci. Lett. 711 (2019) 134387.
[61] J. Cheng, Y. Zhen, S. Miksys, D. Beyoglu, K.W. Krausz, R.F. Tyndale, A. Yu, J.R. Idle, F.J. Gonzalez, Potential role of CYP2*D6* in the central nervous system, Xenobiotica; Fate Foreign Compd. Biol. Syst. 43 (11) (2013) 973–984.
[62] L.K. Chico, H.A. Behanna, W. Hu, G. Zhong, S.M. Roy, D.M. Watterson, Molecular properties and CYP2*D6* substrates: central nervous system therapeutics case study and pattern analysis of a substrate database, Drug Metabol. Disposit.: Biol. Fate Chem. 37 (11) (2009) 2204–2211.
[63] D. Dolles, M. Hoffmann, S. Gunesch, O. Marinelli, J. Moller, G. Santoni, A. Chatonnet, M.J. Lohse, H.J. Wittmann, A. Strasser, M. Nabissi, T. Maurice, M. Decker, Structure-activity relationships and computational investigations into the development of potent and balanced dual-acting butyrylcholinesterase inhibitors and human cannabinoid receptor 2 ligands with pro-cognitive in vivo profiles, J. Med. Chem. 61 (4) (2018) 1646–1663.
[64] T. Maurice, B.P. Lockhart, A. Privat, Amnesia induced in mice by centrally administered beta-amyloid peptides involves cholinergic dysfunction, Brain Res. 706 (2) (1996) 181–193.
[65] S. Kumar, A. Singh, K. Kumar, V. Kumar, Recent insights into synthetic beta-carbolines with anti-cancer activities, Eur. J. Med. Chem. 142 (2017) 48–73.
[66] S.A. Hudson, H. Ecroyd, T.W. Kee, J.A. Carver, The thioflavin T fluorescence assay for amyloid fibril detection can be biased by the presence of exogenous compounds, FEBS J. 276 (20) (2009) 5960–5972.
[67] G.L. Ellman, K.D. Courtney, V. Andres Jr., R.M. Feather-Stone, A new and rapid colorimetric determination of acetylcholinesterase activity, Biochem. Pharmacol. 7 (1961) 88–95.
[68] P.C. Chen, W.J. Tsai, Y.F. Ueng, T.T. Tzeng, H.L. Chen, P.R. Zhu, C.H. Huang, Y.J. Shiao, W.T. Li, Neuroprotective and antineuroinflammatory effects of hydroxyl-functionalized stilbenes and 2-arylbenzo[b]furans, J. Med. Chem. 60 (9) (2017) 4062–4073.
[69] T. Mosmann, Rapid colorimetric assay for cellular growth and survival: application to proliferation and cytotoxicity assays, J. Immunol. Methods 65 (1–2) (1983) 55–63.
[70] D.S. Yoon, M.H. Lee, D.S. Cha, Measurement of intracellular ROS in caenorhabditis elegans using 2',7'-dichlorodihydrofluorescein diacetate, Bio-protocol 8 (6) (2018).
[71] H.J. Ha, D.W. Kang, H.M. Kim, J.M. Kang, J. Ann, H.J. Hyun, J.H. Lee, S.H. Kim, H. Kim, K. Choi, H.S. Hong, Y. Kim, D.G. Jo, J. Lee, J. Lee, Discovery of an orally bioavailable benzofuran analogue that serves as a beta-amyloid aggregation inhibitor for the potential treatment of Alzheimer's disease, J. Med. Chem. 61 (1) (2018) 396–402.
[72] X. Shi, X. Lu, L. Zhan, L. Liu, M. Sun, X. Gong, H. Sui, X. Niu, S. Liu, L. Zheng, J. Chen, Y. Zhou, Rat hippocampal proteomic alterations following intrahippocampal injection of amyloid beta peptide (1–40), Neurosci. Lett. 500 (2) (2011) 87–91.
[73] D.S. Weitzner, E.B. Engler-Chiurazzi, L.A. Kotilinek, K.H. Ashe, M.N. Reed, Morris water maze test: optimization for mouse strain and testing environment, J. Visual. Exp.: JoVE 100 (2015) e52706.
[74] H. Darwish, H. Hasan, Y-shaped maze to test spontaneous object recognition and temporal order memory after traumatic brain injury, Methods Mol. Biol. 2011 (2019) 383–392.
[75] R. Cao, Q. Chen, X. Hou, H. Chen, H. Guan, Y. Ma, W. Peng, A. Xu, Synthesis, acute toxicities, and antitumor effects of novel 9-substituted beta-carboline derivatives, Bioorg. Med. Chem. 12 (17) (2004) 4613–4623.